Telomeric C-circles localize at nuclear pore complexes in Saccharomyces cerevisiae

Paula Aguilera, Marion Dubarry, Julien Hardy, Michael Lisby, Marie-Noëlle Simon, Vincent Géli

Telomeric C-circles localize at Nuclear Pore Complexes in *Saccharomyces cerevisiae*

Paula Aguilera[#1,2], Marion Dubarry[#1], Julien Hardy[1], Michael Lisby[3], Marie-Noëlle Simon[1,*] and Vincent Géli[1,*]

[1]Marseille Cancer Research Center (CRCM), U1068 Inserm, UMR7258 CNRS, Aix Marseille University, Institut Paoli-Calmettes, 27 bd Leï Roure, Marseille, France. Equipe labellisée Ligue.

[2]Present address: Centro Andaluz de Biología Molecular y Medicina Regenerativa (CABIMER), Consejo Superior de Investigaciones Científicas (CSIC) - Universidad de Sevilla - Universidad Pablo de Olavide, Seville, Spain.

[3]Department of Biology, University of Copenhagen, DK-2200 Copenhagen N, Denmark

# these authors contributed equally to this work

*Correspondence: marie-noelle.simon@inserm.fr and vincent.geli@inserm.fr

Keywords: Alternative Lengthening of Telomeres, senescence, C-circles, telomeres, recombination

ABSTRACT

As in human cells, yeast telomeres can be maintained in cells lacking telomerase activity by recombination-based mechanisms known as ALT (Alternative Lengthening of Telomeres). A hallmark of ALT human cancer cells are extrachromosomal telomeric DNA elements called C-circles, whose origin and function have remained unclear. Here, we show that extrachromosomal telomeric C-circles in yeast can be detected shortly after senescence crisis and concomitantly with the production of survivors arising from "type II" recombination events. We uncover that C-circles bind to the nuclear pore complex (NPC) and to the SAGA-TREX2 complex, similar to other non-centromeric episomal DNA. Disrupting the integrity of the SAGA/TREX2 complex affects both C-circle binding to NPCs and type II telomere recombination, suggesting that NPC tethering of C-circles facilitates formation and/or propagation of the long telomere repeats characteristic of type II survivors. Furthermore, we find that disruption of the nuclear diffusion barrier impairs type II recombination. These results support a model in which concentration of C-circles at NPCs benefits type II telomere recombination, highlighting the importance of spatial coordination in ALT-type mechanisms of telomere maintenance.

67

68 **INTRODUCTION**

69

70 Telomeres at the ends of linear chromosomes are designed for protection against DNA
71 degradation, chromosome fusion and homologous recombination. They form nucleoprotein
72 structures composed of G-rich repeated sequences ending with a 3' single-strand overhang
73 and coated by a complex of proteins called shelterin (Ruis & Boulton, 2021). In
74 *Saccharomyces cerevisiae*, telomeres consist of about 300bp of TG_{1-3} repeats, ending with a
75 3' single-strand overhang of 10-15 nucleotides (Wellinger *et al*, 1993). The double-strand
76 telomeric DNA is bound by Rap1 that, together with Rif1 and Rif2, plays a central role in
77 telomere capping, while Cdc13 binds specifically to the single-strand 3'-overhang (Kupiec,
78 2014). As in mammals, telomere length homeostasis is dependent on the activity and
79 regulation of the telomerase, which is constitutively expressed in yeast.

80 In metazoans, telomerase expression is usually turned off during embryogenesis and
81 most of somatic cells do not express telomerase or do it at suboptimal level (Wright *et al*,
82 1996). In the absence of telomerase, telomeres shorten with each cell division until they reach
83 a critical length that prevents efficient capping and induces a permanent cell cycle arrest
84 called replicative senescence (Di Micco *et al*, 2021). Replicative senescence acts as a potent
85 tumor suppressor mechanism as tumor cells need to maintain functional telomeres to
86 proliferate continuously (Kim *et al*, 1994). Although most cancer cells accumulate mutation
87 leading to *de novo* expression of the telomerase, some of them use homologous
88 recombination (HR) to reconstitute functional, long telomeres in a process called Alternative
89 Lengthening of telomeres (ALT) (Shay *et al*, 2012).

90 Inactivation of telomerase in *S. cerevisiae* leads to severe telomere erosion in about 50
91 generations. Eroded dysfunctional telomeres initiate a Mec1-dependent checkpoint cascade
92 that arrests the cell cycle in G2 phase (Enomoto *et al*, 2002; IJpma & Greider, 2003;
93 Lundblad & Szostak, 1989). This permanent G2/M arrest is defined as crisis at the cell
94 population level. Among the population of senescent cells, few are able to recover functional
95 telomeres through HR and hence to escape cell cycle arrest (Lundblad & Blackburn, 1993).
96 Two types of survivors have been described in *S. cerevisiae* (Chen *et al*, 2001; Le *et al*,
97 1999). Type I survivors show amplification of the Y' subtelomeric region while maintaining
98 short terminal telomere repeats. They are dependent on the Rad52 and Rad51 recombination
99 factors. Type II survivors, which display very long and heterogeneous terminal telomere
100 repeats depend on the recombination proteins Rad52 and Rad59 (Chen *et al*, 2001) as well as

101 the Mre11-Rad50-Xrs2 complex (Tsukamoto *et al*, 2001), the helicase Sgs1 (Lee *et al*, 2007)
102 and the nucleases Sae2 and Exo1 (Hardy *et al*, 2014; Maringele & Lydall, 2004). As in ALT
103 tumor cells, maintenance of functional telomeres in both types of survivors depends on the
104 mechanism of break-induced replication (Dilley *et al*, 2016; Lydeard *et al*, 2007; Min *et al*,
105 2017; Roumelioti *et al*, 2016).

106 Although several components implicated in type II recombination have been identified
107 over time (Claussin & Chang, 2015), the molecular transactions leading to type II
108 recombination remain poorly understood. The foremost question is the nature of the template
109 that is used to generate up to 10 kb of telomere repeats in a few generations (Teng & Zakian,
110 1999; Teng *et al*, 2000) at a time when telomere sequences are exhausted at most
111 chromosome ends. The observation that artificial extrachromosomal circles of telomeric DNA
112 (t-circle) can serve as a template for telomere elongation in *K. lactis* (Natarajan &
113 McEachern, 2002) raised the possibility that t-circles might be copied through a rolling circle
114 amplification mechanism to generate the long telomeres characteristics of ALT cells and type
115 II survivors (Cesare & Reddel, 2010; McEachern & Haber, 2006; Kockler *et al*, 2021b). The
116 presence of partially duplexed telomere circles (called C-circles) is indeed the most robust
117 hallmark of human ALT cancer cells (Henson *et al*, 2009). T-circles have also been described
118 in survivors after telomerase inactivation in *S. cerevisiae* (Larrivée & Wellinger, 2006).
119 Spatial localization of the DNA damage is a key determinant in the choice of the
120 pathway used to repair double-strand breaks (Horigome *et al*, 2014). We have previously
121 demonstrated that eroded telomeres that arise in the absence of telomerase are localized to the
122 Nuclear Pore Complexes (NPCs) in *S. cerevisiae* (Khadaroo *et al*, 2009) and that this
123 localization favors type II survivor formation (Churikov *et al*, 2016). In the present study, we
124 asked whether t-circles might also localize to the NPCs during senescence where they might
125 serve as a substrate to either initiate telomere elongation or facilitate its spreading to all
126 telomeres. This hypothesis was incited by the observations that non-centromeric DNA circles
127 attach to the nuclear envelope through the NPCs and the SAGA/TREX2 complex in yeast
128 (Denoth-Lippuner *et al*, 2014; Shcheprova *et al*, 2008).
129 Here, we report detection of C-circles in telomerase-negative yeast cells immediately
130 after the nadir of senescence and concurrently with the first type II recombination events. C-
131 circles interact with the SAGA/TREX2 components Ada2 and Sac3 and co-
132 immunoprecipitate with the nucleoporin Nic96 in an Ada2 and Sus1-dependent manner.
133 Inactivation of SAGA/TREX2 through deletion of *ADA2*, *SUS1* or *SAC3* in telomerase-

134 negative cells impaired the production of survivors suggesting that the localization of C-
135 circles to the NPCs plays a role in the formation of type II telomeres. Finally, we showed that
136 inactivation of the nuclear diffusion barrier that restrains the segregation of non-centromeric
137 episomes to the daughter cell (Baldi *et al*, 2017; Denoth-Lippuner *et al*, 2014; Shcheprova *et*
138 *al*, 2008), also impairs the formation of type II survivors. This raises the possibility that C-
139 circles need to concentrate in one cell for fully efficient type II recombination. Altogether, our
140 data point out that efficient type II recombination might require spatial coordination between
141 eroded telomeres and the template for its repair.
142
143 **RESULTS**
144 **Telomeric circles are produced during senescence at the time of type II survivor**
145 **formation**
146 To detect telomeric circles in *S. cerevisiae* during replicative senescence, we adapted in yeast
147 the Rolling Circle Amplification (RCA) assay previously developed in human cells (Henson
148 *et al*, 2009). The *in vitro* RCA assay is based on the auto-primed production of a long single-
149 strand DNA using the Φ29 polymerase through a rolling circle mechanism starting with either
150 partially double-stranded or a nicked DNA circle (**Fig 1A**). Haploid *est2*Δ clones were
151 isolated by micromanipulation on plates of the spores originated from a heterozygous
152 *est2*Δ*/EST2* diploid. The clones were next propagated in liquid cultures for ten days (about
153 120 population doublings) via serial dilutions every 24 hours as previously described
154 (Churikov *et al*, 2014) **(Fig 1B)**. The growth capacity of the clonal cell populations was
155 assessed by measurement of the cell density every day. As expected, the growth of the *est2*Δ
156 clones progressively declined, in a course of five days on average, until they went through a
157 telomere-erosion driven crisis and formed survivors **(Fig 1C)**. In liquid culture, type II
158 survivors have a growth advantage over type I survivors and outcompete them completely
159 after a single dilution (**Fig 1C, middle panel**). RCA assays were performed on DNA samples
160 prepared at the different time points of the senescence. The product of the RCA assay was
161 loaded to a membrane using a dot blotter and the RCA product was detected by hybridization
162 with a telomeric probe in native conditions to detect only the RCA single-strand DNA
163 product. No signal was detected before the nadir of senescence, however a strong signal of
164 Φ29-dependent amplification was observed at later time points in parallel with the appearance
165 of type II survivors (**Fig 1C and Appendix Fig S1A)**. The RCA signal persisted when
166 survivors were maintained in liquid culture for up to 8 days (about 80 population doublings),
167 suggesting a recurrent production of t-circles (**Appendix Fig S1B)**. Reintroduction of *EST2* in

168 *est2*Δ type II survivors did not abolish the RCA signal **(Appendix Fig S1C)**. This suggests
169 that t-circles are byproducts of recombination at telomeres and possibly are generated during
170 their replication as it has been proposed for ALT cancer cells (Zhang *et al*, 2019).
171 To further confirm that the signal was specific to the product of t-circle amplification,
172 the RCA reactions were loaded on a denaturing gel (**Fig 1D**). As expected, the single-stranded
173 DNA amplification product was detected close to the wells, as previously described (Henson
174 *et al*, 2009; Vannier *et al*, 2012). This result confirmed that the dot blot analysis did not detect
175 the presence of linear single-stranded repeats at chromosome ends but only the product of
176 RCA amplification. Finally, the dot blot signals dropped upon treatment of the RCA product
177 with the exonuclease *Exo*VII (**Fig 1E**) further validating that the signals reflect the production
178 of single-strand DNA by the Φ29 polymerase templated by extrachromosomal circles. Since
179 no exogenous primer was provided in the reaction, the t-circles that serve as substrate for the
180 RCA reaction could be either partially or completely duplexed with a nick in the G-rich
181 strand. Together our results show that partially single-stranded t-circles can be detected
182 shortly after crisis in the absence of telomerase and this correlates with the emergence of type
183 II survivors.
184
185 **Telomeric circles are partially duplexed DNA-DNA specific to type II survivors**
186 We next wondered about the structure of the telomeric circles produced in *S. cerevisiae*. The
187 RCA products hybridized with a telomeric CA oligonucleotide complementary to the G-rich
188 telomere sequence, but not with the corresponding GT probe (**Fig 2A**). No signal was
189 detected with a Y' subtelomeric probe signifying that the t-circles did not include
190 subtelomeric sequences **(Fig 2A)**. Accordingly, RCA products were detected even in the
191 absence of dCTP and dATP in the reaction mixture showing that at least some circles contain
192 only telomeric repeats **(Fig 2B)**. Thus, we concluded that the t-circle backbone is formed by
193 the C-rich strand of the telomeric sequence (C-circles). Adding a telomeric primer to the RCA
194 reaction did not enhance the signal **(Appendix Fig S2)**. To further determine whether fully
195 single-stranded t-circles are also present, the DNA sample was treated with exonuclease *Exo*I
196 to degrade linear single-stranded DNA and with a duplex-specific nuclease (DSN) that
197 specifically degrades double-stranded DNA (**Appendix Fig S2A**). RCA was then performed
198 after addition of either CA or TG telomeric oligonucleotides to prime the reaction. No
199 amplification was detected suggesting that type II survivors do not contain DNA circles that
200 are entirely single-stranded **(Appendix Fig S2B)**. We were unable to conclude on the

201 presence of telomeric circles carrying a nick on each DNA strand as such circles are not
202 appropriate substrates for RCA.
203 To determine whether C-circles are specific to type II survivors, we monitored their
204 presence in *rad59Δ est2Δ* and *rad51Δ est2Δ* cells during the course of senescence and
205 survivor production. C-circles were not detected in *rad59Δ est2Δ* cells that form only type I
206 survivors (**Fig EV1A**) but were present in *rad51Δ est2Δ* cells concomitant with the
207 appearance of type II survivors (**Fig EV1B**). Although we cannot exclude a direct role of
208 Rad59, this result is consistent with a tight link between the presence of C-circles and type II
209 recombination.
210 Because telomere recombination during senescence is enhanced by TERRA
211 transcription and the presence of R-loops at telomeres (Balk *et al*, 2013; Yu *et al*, 2014; Graf
212 *et al*, 2017), we questioned whether C-circles are DNA/RNA hybrids. Prolonged incubation
213 of the DNA samples with high concentrations of RNaseA or RNaseH before RCA assay did
214 not prevent RCA product formation **(Fig EV2A and B)**. Furthermore, overexpression of
215 *RNH1* in *est2*Δ cells during the course of senescence did not prevent the production of C-
216 circles in type II survivors **(Fig EV2C)**.
217 Taken together, our data showed that *S. cerevisiae* type II survivors carry C-circles similar to
218 those found in human ALT cancer cells (Henson *et al*, 2009).
219
220 **C-circles bind to the Nuclear Pore Complexes**
221 We next addressed the possibility that C-circles localize or are enriched at the NPCs as
222 previously reported for other types of extrachromosomal DNA circles (Shcheprova *et al*,
223 2008). To this purpose, we used the nucleoporin Nic96, which is part of the inner ring of the
224 NPCs, to set up the C-circles co-IP experiment. We isolated independent haploid *est2*Δ
225 *Nic96-RFP* cells from a heterozygous diploid as described above and propagated them in
226 liquid culture until the appearance of type II survivors (**Fig 3A and Appendix Fig S3A**).
227 *est2*Δ clones isolated from the same diploid were used as a control showing that the *NIC96-*
228 *RFP* allele did not impact the kinetics of senescence and the capacity of *est2*Δ cells to form
229 type II survivors **(Fig 3A and B)**. Type II survivor cells either expressing or not Nic96-RFP
230 were fixed with para-formaldehyde and the NPCs were immunoprecipitated from cell
231 extracts. After crosslink reversal, RCA assays were performed on the purified DNA that co-
232 immunoprecipitated with Nic96-RFP. No C-circles were detected in immunoprecipitates from
233 either telomerase positive control cells expressing Nic96-RFP or in *est2*Δ cells with untagged

234 Nic96 (**Fig 3C**). In contrast, Nic96-RFP immunoprecipitates from type II survivors displayed
235 RCA signal **(Fig. 3C and D)**.
236 The NPC-associated complex TREX2 and the transcriptional co-activator SAGA are
237 part of the gene gating mechanism that couples transcription and mRNA export (García-
238 Oliver *et al*, 2012). SAGA-TREX2 is also implicated in the retention of extrachromosomal
239 DNA circles at the NPCs (Denoth-Lippuner *et al*, 2014). We previously reported that deletion
240 of *ADA2*, a component of the SAGA complex, impairs survivor formation with some *est2*Δ
241 *ada2*Δ clones either unable to form type II survivors or being greatly delayed in producing
242 them (Churikov *et al*, 2016). Deletion of *ADA2* did not prevent the production of C-circles in
243 *est2*Δ cells when they eventually formed type II survivors. The same holds true for the
244 deletion of *SAC3*, a component of the TREX2 complex and the deletion of *SUS1*, which is
245 part of both the SAGA and TREX2 complexes **(Appendix Fig S3B)** suggesting that
246 SAGA/TREX2 is not required for the production of the circles *per se*. We thus asked whether
247 the localization of C-circles to the NPCs depends on SAGA/TREX2. We observed a
248 significant drop of C-circle amplification in Nic96-RFP immunoprecipitates in type II
249 survivors arising from the *est2*Δ *ada2*Δ and *est2*Δ *sus1*Δ clones **(Figs 3D and E, Figs EV3A**
250 **and B)** suggesting that retention of C-circles at the NPCs requires a functional SAGA/TREX2
251 complex.
252
253 **C-circles bind to SAGA/TREX2 complexes**
254 We next asked if SAGA/TREX2 components interact with C-circles. The C-circles co-IP
255 assay followed by RCA was conducted in type II survivors expressing a Myc-tagged Ada2.
256 For that, *est2*Δ *ADA2*-Myc clones isolated from a heterozygous diploid were propagated in
257 liquid cultures until the formation of type II survivors (**Fig 4A and B**) and RCA assays were
258 performed on DNA immunoprecipitated with Ada2-Myc. C-circles were detected exclusively
259 in the immunoprecipitates from type II survivors expressing Ada2-Myc (**Fig. 4C and D**). To
260 demonstrate that the signal on the dot blots results from amplification of the C-circles and not
261 of the long terminal repeats present in type II survivors, products of the RCA reaction were
262 separated by denaturing agarose gel electrophoresis. As expected, the long single-stranded
263 DNA produced by the amplification of C-circles with the Φ29 polymerase was detected close
264 to the wells while no gross amplification of the chromosomal terminal repeats was detected
265 (**Fig EV3C**). Remarkably, C-circles also co-immunoprecipitated with Sac3 (**Fig EV3D**).
266 Together these data suggest that C-circles produced slightly before or during type II

recombination localize to the NPCs through interaction with the SAGA/TREX2 complex as described for other non-centromeric episomes (Denoth-Lippuner *et al*, 2014).

SAGA/TREX2 favors type II recombination

We next addressed whether TREX2 inactivation also impacts type II recombination. *SUS1* and *SAC3* deletions were combined to *est2*Δ as described above, and liquid senescence assays were conducted with several independent *est2*Δ *sus1*Δ and *est2*Δ *sac3*Δ clones **(Fig 5A, B and Appendix Fig S4)**. The deletion of *SUS1* extended the crisis period to the extent similar to that of *ADA2* (Churikov *et al*, 2016), indicating that formation of survivors was compromised in *est2*Δ *sus1*Δ cells **(Fig 5C)**. Accordingly, telomere length analysis by Southern blot of individual clones showed that *sus1*Δ impaired type II survivor formation (**Fig 5D and Appendix Fig S5**). The delay in forming survivors was much more pronounced in *est2*Δ *sac3*Δ cells as compared to *est2*Δ *ada2*Δ and *est2*Δ *sus1*Δ cells (**Fig. 5C**). However, type II survivors were eventually detected at late time points in most of the clones that were analyzed (**Fig 5D and Appendix Fig S6**). The prolonged crisis in the absence of Sac3 suggests that its deletion also affects type I survivor formation leaving more time for the cells to perform type II recombination even though its efficiency is decreased. In favor of this possibility, Sac3 is a scaffold protein with three regions that interact with various partners including Sus1 (Gordon *et al,* 2017).

As mentioned above, the SAGA complex acts as a transcriptional co-activator that plays a role genome-wide (Bonnet *et al*, 2014) and TREX2 mediates the anchoring of transcribed genes to the NPCs through a direct interaction between Nup1 and Sac3 (Jani *et al*, 2014) to favor mRNA export (Fischer *et al*, 2002; Rodríguez-Navarro *et al*, 2004). Furthermore, inactivation of TREX2 components interferes with transcription of long GC-rich genes and induces high levels of recombination consecutive to conflicts between the replication and transcription machineries (Santos-Pereira *et al*, 2014). Because of the role of TERRA in telomere recombination (Balk *et al*, 2013), we addressed the possibility that the defect of type II survivor formation observed in SAGA/TREX2 mutant relies on TERRA metabolism. RT-qPCR analysis of TERRA RNA production at single telomeres during the course of senescence and survivor formation did not reveal a defect of TERRA transcription in *est2*Δ *ada2*Δ as compared to *est2*Δ control cells **(Fig EV4A and B)**. Thus, it seems unlikely that the failure of type II formation observed in *est2*Δ *ada2*Δ cells resulted from an alteration of TERRA-induced recombination.

300 Previously we showed that recombinogenic eroded telomeres localize to the NPCs
301 (Churikov *et al*, 2014, 2016). Potentially, TREX2-dependent gene gating of the transcribed
302 telomeres could contribute to their localization to the NPCs. Therefore, we monitored the
303 localization of dysfunctional telomeres detected by colocalization of Cdc13-YFP and Rad52-
304 RFP (**Fig EV4C).** Cdc13-YFP/Rad52-RFP foci localized to the NPC marked by CFP-Nup49
305 in *est2*Δ *ada2*Δ cells **(Fig EV4C),** excluding the possibility that gene gating through TREX2
306 participates in the relocalization of eroded telomeres.
307 Overall, these data suggest that the defect in survivor formation observed upon
308 inactivation of the SAGA/TREX2 complex is linked to its role in tethering C-circles to the
309 NPCs and that this function may facilitate the formation and/or propagation of type II
310 survivors.
311
312 **Inactivation of components of the nuclear diffusion barrier impairs type II**
313 **recombination**
314 Although long controversial, it is now clear that retention of at least a subset of NPCs in the
315 mother cell during anaphase is part of the mechanisms leading to the accumulation of
316 extrachromosomal ribosomal circles (ERCs) with age (Denoth-Lippuner *et al*, 2014; Gehlen
317 *et al*, 2011; Khmelinskii *et al*, 2011; Shcheprova *et al*, 2008). Localization of the C-circles to
318 the NPCs raised a possibility that fully efficient type II survivor formation and/or propagation
319 might depend on the nuclear diffusion barrier (NDB). In this scenario, the NDB would help to
320 reach a threshold level of C-circles necessary to facilitate their interaction with the eroded
321 telomeres that transiently relocalize to the NPCs. To challenge this hypothesis, we evaluated
322 the capacity of the NDB mutants to produce type II survivors. Two proteins with known
323 function in NDB are Shs1 and Bud6, a septin localized at the mother bud neck and an actin
324 binding protein, respectively (Shcheprova *et al*, 2008). Deletions of *SHS1* and *BUD6* were
325 combined to *est2*Δ and *est1*Δ respectively and liquid senescence assays conducted with
326 several independently isolated clones as previously described **(Fig 6A and B, Appendix Fig**
327 **S7)**. The deletions of *SHS1* and *BUD6* extended the crisis period indicating a defect in
328 survivor formation **(Fig 6C)**. Accordingly, telomere length analysis by Southern blot revealed
329 a defect in type II survivor formation upon inactivation of either Shs1 or Bud6 **(Fig 6D,**
330 **Appendix Figs S8-9).**
331 It has recently been demonstrated that the extended lifespan observed in yeast upon
332 mild temperature stress results from the downregulation of the nuclear diffusion barrier and
333 hence relaxation of the retention of DNA circles in the mother cell (Baldi *et al*, 2017).

334 Strikingly, performing a parallel senescence assay at 30°C and 37°C on *est2*Δ cells issued
335 from the same spore showed that elevated temperature not only accelerated senescence but
336 also dramatically interfered with type II recombination **(Fig EV5A and B).**
337
338 **DISCUSSION**
339
340 Extrachromosomal circular DNAs from chromosomal origin are common in yeast and human
341 cells (Møller *et al*, 2018, 2015; Qiu *et al*, 2021). However, how they are produced and
342 whether they interfere with DNA metabolism or DNA damage repair remain elusive. One best
343 studied examples is the extrachromosmal ribosomal DNA circles that arise from
344 recombination between the rDNA repeats and accumulate in the mother cells where they
345 contribute to aging (Sinclair & Guarente, 1997). This asymmetric segregation of ERCs at
346 anaphase relies on both the binding of ERCs to the NPCs and the nuclear diffusion barrier
347 that is thought to limit the diffusion of the NPC-bound circles into the bud (Baldi *et al*, 2017;
348 Denoth-Lippuner *et al*, 2014; Shcheprova *et al*, 2008). Extrachromosomal circles are also a
349 hallmark of ALT cancer cells that maintain functional telomeres through recombination
350 instead of telomerase activity (Henson *et al*, 2009). The most abundant telomeric circles in
351 ALT cells are composed of partially duplexed C-rich strand (C-circles) that might be
352 byproducts of the repair of the DNA replication forks stalled in long telomere sequences
353 (Henson *et al*, 2009; Rivera *et al*, 2017). Here, we show that C-circles are also produced in *S.*
354 *cerevisiae* at the time of type II survivor formation. The presence of t-circles has already been
355 revealed in type II survivors using 2D-gel analysis (Larrivée & Wellinger, 2006; Lin *et al*,
356 2005). However, although this approach detected partially double-stranded circles, these
357 circles contained the G-rich rather than C-rich strand (Larrivée & Wellinger, 2006). We did
358 not detect G-circles using the RCA assay. This suggests that G-circles might be nicked on
359 both strands preventing their amplification by the Φ29 polymerase. A single-stranded TG-rich
360 telomeric probe has not been used in this founding study likely explaining why the C-circles
361 described here were not detected by 2D-gel electrophoresis. The mechanism of C-circle
362 production remains elusive. It has been proposed that they arise from processing of DNA
363 structures generated upon replication stress (Rivera *et al*, 2017). Accordingly, telomeres are
364 an obstacle to replication fork progression in both yeast and mammals (Özer *et al*, 2018;
365 Simon *et al*, 2016; Bonnell *et al*, 2021).
366 Here, we show that C-circles in yeast localize to the NPCs in a pathway dependent on
367 the SAGA/TREX2-components Ada2 and Sus1. We cannot exclude that this pathway is part

368 of a detoxification process as it has been suggested for ERCs (Shcheprova *et al*, 2008;
369 Sinclair & Guarente, 1997). Alternatively and not exclusively, we propose that retention of C-
370 circles at the NPCs might be part of the process that ultimately results in the production of
371 type II survivors. We have previously shown that in the absence of telomerase, eroded
372 telomeres bound by SUMOylated proteins are recognized by the SUMO-targeted ubiquitin
373 ligase Slx5-Slx8 and relocate to the NPCs (Khadaroo et al., 2009). Relocalization to the NPCs
374 favors type II survivor recombination, which involves BIR although the identity of the
375 template used to produce elongated telomeres remains elusive (Churikov *et al*, 2016;
376 McEachern & Haber, 2006). We propose that C-circles may provide a template for telomere
377 elongation through single strand annealing and rolling circle amplification **(Fig 7)** as it has
378 been suggested in the yeast *K. lactis* (McEachern & Haber, 2006). In this hypothesis, the
379 proximity of eroded telomeres and C-circles at the NPCs would spatially favor their
380 interaction and hence telomere elongation. In line with this possibility, our data show that
381 inactivation of SAGA/TREX2 components impacts type II recombination.
382 Unfortunately we were unable to detect C-circles before the detection of the first type
383 II recombination events. This prevented us to directly test our model and to determine the
384 genetic requirements for the formation of C-circles. This may be due to technical constraints
385 related to the fact that the C-circles would be below the threshold of RCA detection in the
386 population of senescing cells of which only a few (on average one in 10^5 cells) succeed in
387 restoring their telomeres via recombination and become type II survivors (McEachern &
388 Haber, 2006, Kockler *et al*, 2021a). Alternatively, C-circles might be produced during the
389 first recombination events that generate long telomeres and then used to facilitate spreading of
390 telomere repeats to other eroded telomeres. In line with this possibility, it has been recently
391 proposed that the production of type II survivors might involve mixed BIR processes, each
392 with specific genetic requirements (Kockler *et al*, 2021a, 2021b). It is conceivable that this
393 complexity actually reflects different stages of survivor maturation, from the elongation of
394 one or a few telomeres to the regeneration of a complete set of functional telomeres allowing
395 resumption of growth, and finally to the maintenance of telomeres recurrently dependent on
396 HR.
397 Our data also implicate components of the nuclear diffusion barrier in facilitating type
398 II survivor formation. Whether NDB plays its role by concentrating C-circles in the mother
399 cells to facilitate telomere elongation or to facilitate the spreading of telomere repeats among
400 the chromosome ends will need further investigation. It is noteworthy that although
401 maintenance of telomeres through type II recombination affects neither the growth rate nor

402 the genome integrity of the cells, it significantly reduces their replicative life span (Chen *et al*,
403 2009).
404 Overall, our study suggests that formation of the type II survivors depends on multiple
405 spatially organized events with a central role of the NPCs in recruiting both eroded telomeres
406 and C-circles. This multifactorial constrains might explain the very low efficiency of type II
407 survivor formation in *S. cerevisiae* and, by extension, the low frequency of ALT in cancer
408 cells.
409
410
411 **MATERIALS AND METHODS**
412
413 **Yeast strains and primers**
414 Strains and primers used in this study are listed in the Appendix Tables S1 and S2,
415 respectively. All strains were constructed using standard genetic methods.
416
417 **Senescence assays**
418 Senescence assays were performed in liquid culture starting from haploid spores obtained by
419 dissection of the tetrads produced by sporulation of diploid cells heterozygous for *EST2*
420 (*EST2*/*est2Δ*) and for the gene(s) of interest. Diploids obtained by crossing two haploid
421 mutants were grown in YPD plates for about 50 PDs before sporulation to ensure
422 homogeneous telomere length. After dissection, spores were grown for 3 days on plate at
423 30°C (about 25-30 PDs). The entire colonies were inoculated and then propagated in 15 ml of
424 YPD at 30°C via serial dilutions to OD_{600}=0.01 every 24 hours until the appearance of
425 survivors. The duration of the crisis was estimated as the number of days the culture remains
426 at the lowest OD (with no increase in cell density). As soon as the culture gained some
427 growth capacity, even intermediate, we considered that survivors started to appear to avoid
428 any putative side effect of the mutation on the growth rate. Determination of the type of
429 survivors has been done at the second day after stabilization of the growth rate.
430
431 **Telomere Southern blot analysis**
432 Genomic DNA (25µg estimated with a nanodrop) was digested overnight with *Xho*I at 37°C.
433 Digested DNA was resolved in 0.9% agarose gel and transferred onto the nylon membrane
434 (Hybond-XL) in alkaline conditions. The blotted DNA was hybridized with a probe prepared
435 by random priming of the DNA fragment composed of TG_{1-3} repeats in the presence of [α-

436 ^{32}P]dCTP.

437

438 **Chromatin immunoprecipitation**

439 Yeast cells were grown in YPD at 30°C to OD_{600}=1 and fixed at RT for 10 min with 1%
440 formaldehyde (Sigma; F8775). Fixation was quenched with 0.25M glycine for 5 min. After
441 three washes with cold 1x TBS, the cell pellets were frozen and stored at -80°C. Thawed were
442 resuspended in the lysis buffer (50 mM HEPES-KOH pH 7.5, 150 mM NaCl, 1 mM EDTA,
443 1% Triton X-100, 0.1% Na-deoxycholate) containing 1 mM PMSF and a protease inhibitor
444 cocktail (cOmplete tablet, EDTA-free, Roche) and disrupted in a bead-beater for 3x 30 sec at
445 5000rpm (Precellys 24, Bertin). Lysates were cleared by centrifugation (2000xg, 4°C) and
446 supernatants were collected. Aliquotes were saved to check the protein level and for RCA
447 experiments (Inputs). The cleared lysates were then incubated with either a mouse
448 monoclonal anti-Myc 9E10 antibody (Santa Cruz Biotechnology, sc-40) or a rabbit polyclonal
449 anti-pHis-mCherry antibody (Home-made) for 2 h 30 min at 4°C. Magnetic Dynabeads
450 Protein G (Invitrogen Dynal AS, Oslo, Norway) were then added for another 2 h 30 min
451 incubation at 4°C. The beads were washed consecutively with lysis buffer, lysis Buffer + 500
452 mM NaCl, Wash Buffer (10 mM Tris-HCl pH 8, 250 mM LiCl, 0.5% NP40, 0.5% Na-
453 deoxycholate, 1 mM EDTA) and with TE 1X. The protein-DNA complexes were eluted from
454 the beads in 1x TE 1% SDS solution. An aliquot of the elution was saved to check the level of
455 the immunoprecipitated proteins. The cross-links were reversed by incubation at 65°C
456 overnight. The samples were treated with proteinase K (Roche) and DNA was purified
457 through phenol-chloroform extraction and resuspended in 25 µl of H2O. The samples were
458 analyzed by RCA assay.

459

460 **RCA assay**

461 2.5 µg of genomic DNA (estimated with a nanodrop) was digested with *PvuII* at 37°C prior
462 Phi29 amplification reaction. For Inputs and co-immunoprecipitated samples, 5µl were used
463 for RCA per condition. For all experiments, samples were incubated with 7.5 U of Φ29
464 polymerase (NEB) in the 1x Φ29 buffer supplemented with 1 mM dNTPs, 0.2 mg/ml BSA,
465 0.1% Tween overnight at 30ºC. The Φ29 polymerase was inactivated 10 min at 65ºC.
466 Samples were diluted with 200 µl 2X SSC and loaded onto 6X SSC-soaked Hybond-XL
467 membrane (GE Healthcare) using a dot blotter. When indicated, the RCA products were
468 loaded on a denaturing 0.8% agarose gel (adapted from Vannier *et al*, 2012) and transferred to

469 a Hybond-XL membrane (GE Healthcare). DNA was UV-crosslinked onto the membrane and
470 hybridized either with the end-labelled single-stranded probes at 37ºC (CA probe: [5'-
471 ^{32}P]CACCACACCCACACACA/GT probe: [5'-^{32}P] TGTGTGTGGGTGTGGTG) or at 55ºC
472 with radiolabelled double-stranded probes. When indicated, treatment with *Exo*VII (NEB)
473 was performed for 4 h at 37ºC to degrade linear ssDNA. Treatment with *Exo*I (NEB) was
474 performed for 1 h at 37ºC followed by *DSN* (NEB) treatment for 2 h at 37ºC. The samples
475 were then denatured and a 3' 2-thio-U primer was added before treatment with Phi29
476 polymerase.
477 Membranes were exposed to a phosphorimager screen and the signal was detected via a
478 Typhoon scanner (GE Healthcare). For co-IP/RCA, quantification was done with the Fiji
479 software by measuring the integrated intensity of the signals. Background signal obtained
480 without Φ29 treatment was subtracted from the Φ29 treated samples. The percentage of the
481 INPUT that was immunoprecipitated was normalized to the *est2*Δ samples. Relative signals
482 were calculated by setting the mean of the *est2*Δ signals from each independent experiment to
483 1. The mean values of the signal for independent clones used in each experiment were
484 represented as a bar graph with the error bars indicating (s.e.m.).
485
486 **TERRA transcription**.
487 Cells were grown in 25 ml of YPD to mid-exponential phase (OD: 0.6-0.8). Total RNA was
488 extracted with hot acidic phenol as described (Graf *et al*, 2017)**.** Three DNase I treatments
489 were done with the RNase-free DNase set from Qiagen to completely remove telomeric DNA
490 from RNA. Reverse transcription was done using 200U of SuperScript III per reaction and
491 TERRA was reverse-transcribed using the CA oligonucleotide as a primer. All primer
492 sequences are listed in Appendix Table S2. TERRA levels were normalized to the *ACT1* RNA
493 levels and converted to relative TERRA expression by normalization to the first time point of
494 the control *est2Δ* strain.
495
496
497 **DATA AVAILABILITY**
498 This study includes no data deposited in external repositories
499
500
501

ACKNOWLEDGMENTS

We thank Brian Luke for the vector overexpressing *RNH1* and Dmitri Churikov for comments on the manuscript. P.A. was supported by the Région Provence-Alpes-Côte d'Azur and the Association pour la Recherche contre le Cancer (ARC). M.D was supported by the Agence Nationale de Recherche (ANR-19-CE12-0023 NIRO). V.G. is supported by the Ligue Nationale Contre le Cancer (Equipe labellisée)

AUTHOR CONTRIBUTION

PA, MD, JH, ML and MNS performed experiments. MNS and VG conceived this study. PA, MD, VG and MNS designed the experiments and discussed the results. MD analyzed the results and contributed to the writing of the manuscript. PA, VG and MNS wrote the manuscript.

CONFLICT OF INTEREST

The authors declare that they have no conflict of interest.

REFERENCES

- Baldi S, Bolognesi A, Meinema AC & Barral Y (2017) Heat stress promotes longevity in budding yeast by relaxing the confinement of age-promoting factors in the mother cell. *eLife* 6
- Balk B, Maicher A, Dees M, Klermund J, Luke-Glaser S, Bender K & Luke B (2013) Telomeric RNA-DNA hybrids affect telomere-length dynamics and senescence. *Nat Struct Mol Biol* 20: 1199–1205
- Bonnell E, Pasquier E & Wellinger RJ (2021) Telomere Replication: Solving Multiple End Replication Problems. *Front Cell Dev Biol* 9: 668171
- Bonnet J, Wang C-Y, Baptista T, Vincent SD, Hsiao W-C, Stierle M, Kao C-F, Tora L & Devys D (2014) The SAGA coactivator complex acts on the whole transcribed genome and is required for RNA polymerase II transcription. *Genes Dev* 28: 1999–2012
- Cesare AJ & Reddel RR (2010) Alternative lengthening of telomeres: models, mechanisms and implications. *Nat Rev Genet* 11: 319–330
- Charifi F, Churikov D, Eckert-Boulet N, Minguet C, Jourquin F, Hardy J, Lisby M, Simon M-N & Géli V (2021) Rad52 SUMOylation functions as a molecular switch that determines a balance between the Rad51- and Rad59-dependent survivors. *iScience* 24: 102231
- Chen Q, Ijpma A & Greider CW (2001) Two survivor pathways that allow growth in the absence of telomerase are generated by distinct telomere recombination events. *Mol Cell Biol* 21: 1819–1827

542 • Chen X-F, Meng F-L & Zhou J-Q (2009) Telomere recombination accelerates cellular
543 aging in Saccharomyces cerevisiae. *PLoS Genet* 5: e1000535
544 • Churikov D, Charifi F, Eckert-Boulet N, Silva S, Simon M-N, Lisby M & Géli V
545 (2016) SUMO-Dependent Relocalization of Eroded Telomeres to Nuclear Pore
546 Complexes Controls Telomere Recombination. *Cell Rep* 15: 1242–1253
547 • Churikov D, Charifi F, Simon M-N & Géli V (2014) Rad59-facilitated acquisition of
548 Y' elements by short telomeres delays the onset of senescence. *PLoS Genet* 10:
549 e1004736
550 • Claussin C & Chang M (2015) The many facets of homologous recombination at
551 telomeres. *Microb Cell Graz Austria* 2: 308–321
552 • Denoth-Lippuner A, Krzyzanowski MK, Stober C & Barral Y (2014) Role of SAGA
553 in the asymmetric segregation of DNA circles during yeast ageing. *eLife* 3
554 • Di Micco R, Krizhanovsky V, Baker D & d'Adda di Fagagna F (2021) Cellular
555 senescence in ageing: from mechanisms to therapeutic opportunities. *Nat Rev Mol*
556 *Cell Biol* 22: 75–95
557 • Dilley RL, Verma P, Cho NW, Winters HD, Wondisford AR & Greenberg RA (2016)
558 Break-induced telomere synthesis underlies alternative telomere maintenance. *Nature*
559 539: 54–58
560 • Enomoto S, Glowczewski L & Berman J (2002) MEC3, MEC1, and DDC2 are
561 essential components of a telomere checkpoint pathway required for cell cycle arrest
562 during senescence in Saccharomyces cerevisiae. *Mol Biol Cell* 13: 2626–2638
563 • Fischer T, Strässer K, Rácz A, Rodriguez-Navarro S, Oppizzi M, Ihrig P, Lechner J &
564 Hurt E (2002) The mRNA export machinery requires the novel Sac3p-Thp1p complex
565 to dock at the nucleoplasmic entrance of the nuclear pores. *EMBO J* 21: 5843–5852
566 • García-Oliver E, García-Molinero V & Rodríguez-Navarro S (2012) mRNA export
567 and gene expression: the SAGA-TREX-2 connection. *Biochim Biophys Acta* 1819:
568 555–565
569 • Gehlen LR, Nagai S, Shimada K, Meister P, Taddei A & Gasser SM (2011) Nuclear
570 geometry and rapid mitosis ensure asymmetric episome segregation in yeast. *Curr*
571 *Biol CB* 21: 25–33
572 • Gordon JMB, Aibara S & Stewart M (2017) Structure of the Sac3 RNA-binding M-
573 region in the Saccharomyces cerevisiae TREX-2 complex. *Nucleic Acids Res* 45:
574 5577–5585
575 • Graf M, Bonetti D, Lockhart A, Serhal K, Kellner V, Maicher A, Jolivet P, Teixeira
576 MT & Luke B (2017) Telomere Length Determines TERRA and R-Loop Regulation
577 through the Cell Cycle. *Cell* 170: 72-85.e14
578 • Hardy J, Churikov D, Géli V & Simon M-N (2014) Sgs1 and Sae2 promote telomere
579 replication by limiting accumulation of ssDNA. *Nat Commun* 5: 5004
580 • Henson JD, Cao Y, Huschtscha LI, Chang AC, Au AYM, Pickett HA & Reddel RR
581 (2009) DNA C-circles are specific and quantifiable markers of alternative-
582 lengthening-of-telomeres activity. *Nat Biotechnol* 27: 1181–1185
583 • Horigome C, Oma Y, Konishi T, Schmid R, Marcomini I, Hauer MH, Dion V, Harata
584 M & Gasser SM (2014) SWR1 and INO80 chromatin remodelers contribute to DNA
585 double-strand break perinuclear anchorage site choice. *Mol Cell* 55: 626–639
586 • IJpma AS & Greider CW (2003) Short telomeres induce a DNA damage response in
587 Saccharomyces cerevisiae. *Mol Biol Cell* 14: 987–1001
588 • Jani D, Valkov E & Stewart M (2014) Structural basis for binding the TREX2
589 complex to nuclear pores, GAL1 localisation and mRNA export. *Nucleic Acids Res*
590 42: 6686–6697

591 • Khadaroo B, Teixeira MT, Luciano P, Eckert-Boulet N, Germann SM, Simon MN,
592 Gallina I, Abdallah P, Gilson E, Géli V, *et al* (2009) The DNA damage response at
593 eroded telomeres and tethering to the nuclear pore complex. *Nat Cell Biol* 11: 980–
594 987
595 • Khmelinskii A, Meurer M, Knop M & Schiebel E (2011) Artificial tethering to
596 nuclear pores promotes partitioning of extrachromosomal DNA during yeast
597 asymmetric cell division. *Curr Biol CB* 21: R17-18
598 • Kim NW, Piatyszek MA, Prowse KR, Harley CB, West MD, Ho PL, Coviello GM,
599 Wright WE, Weinrich SL & Shay JW (1994) Specific association of human
600 telomerase activity with immortal cells and cancer. *Science* 266: 2011–2015
601 • Kockler ZW, Comeron JM & Malkova A (2021a) A unified alternative telomere-
602 lengthening pathway in yeast survivor cells. *Mol Cell* 81: 1816-1829.e5
603 • Kockler ZW, Osia B, Lee R, Musmaker K & Malkova A (2021b) Repair of DNA
604 Breaks by Break-Induced Replication. *Annu Rev Biochem*
605 • Kupiec M (2014) Biology of telomeres: lessons from budding yeast. *FEMS Microbiol*
606 *Rev* 38: 144–171
607 • Larrivée M & Wellinger RJ (2006) Telomerase- and capping-independent yeast
608 survivors with alternate telomere states. *Nat Cell Biol* 8: 741–747
609 • Le S, Moore JK, Haber JE & Greider CW (1999) RAD50 and RAD51 define two
610 pathways that collaborate to maintain telomeres in the absence of telomerase. *Genetics*
611 152: 143–152
612 • Lee JY, Kozak M, Martin JD, Pennock E & Johnson FB (2007) Evidence that a RecQ
613 helicase slows senescence by resolving recombining telomeres. *PLoS Biol* 5: e160
614 • Lin C-Y, Chang H-H, Wu K-J, Tseng S-F, Lin C-C, Lin C-P & Teng S-C (2005)
615 Extrachromosomal telomeric circles contribute to Rad52-, Rad50-, and polymerase
616 delta-mediated telomere-telomere recombination in Saccharomyces cerevisiae.
617 *Eukaryot Cell* 4: 327–336
618 • Lundblad V & Blackburn EH (1993) An alternative pathway for yeast telomere
619 maintenance rescues est1- senescence. *Cell* 73: 347–360
620 • Lundblad V & Szostak JW (1989) A mutant with a defect in telomere elongation leads
621 to senescence in yeast. *Cell* 57: 633–643
622 • Lydeard JR, Jain S, Yamaguchi M & Haber JE (2007) Break-induced replication and
623 telomerase-independent telomere maintenance require Pol32. *Nature* 448: 820–823
624 • Maringele L & Lydall D (2004) EXO1 plays a role in generating type I and type II
625 survivors in budding yeast. *Genetics* 166: 1641–1649
626 • McEachern MJ & Haber JE (2006) Break-induced replication and recombinational
627 telomere elongation in yeast. *Annu Rev Biochem* 75: 111–135
628 • Min J, Wright WE & Shay JW (2017) Alternative Lengthening of Telomeres
629 Mediated by Mitotic DNA Synthesis Engages Break-Induced Replication Processes.
630 *Mol Cell Biol* 37
631 • Møller HD, Mohiyuddin M, Prada-Luengo I, Sailani MR, Halling JF, Plomgaard P,
632 Maretty L, Hansen AJ, Snyder MP, Pilegaard H, *et al* (2018) Circular DNA elements
633 of chromosomal origin are common in healthy human somatic tissue. *Nat Commun* 9:
634 1069
635 • Møller HD, Parsons L, Jørgensen TS, Botstein D & Regenberg B (2015)
636 Extrachromosomal circular DNA is common in yeast. *Proc Natl Acad Sci U S A* 112:
637 E3114-3122
638 • Natarajan S & McEachern MJ (2002) Recombinational telomere elongation promoted
639 by DNA circles. *Mol Cell Biol* 22: 4512–4521

640 • Özer Ö, Bhowmick R, Liu Y & Hickson ID (2018) Human cancer cells utilize mitotic
641 DNA synthesis to resist replication stress at telomeres regardless of their telomere
642 maintenance mechanism. *Oncotarget* 9: 15836–15846
643 • Qiu G-H, Zheng X, Fu M, Huang C & Yang X (2021) The decreased exclusion of
644 nuclear eccDNA: From molecular and subcellular levels to human aging and age-
645 related diseases. *Ageing Res Rev* 67: 101306
646 • Rivera T, Haggblom C, Cosconati S & Karlseder J (2017) A balance between
647 elongation and trimming regulates telomere stability in stem cells. *Nat Struct Mol Biol*
648 24: 30–39
649 • Rodríguez-Navarro S, Fischer T, Luo M-J, Antúnez O, Brettschneider S, Lechner J,
650 Pérez-Ortín JE, Reed R & Hurt E (2004) Sus1, a functional component of the SAGA
651 histone acetylase complex and the nuclear pore-associated mRNA export machinery.
652 *Cell* 116: 75–86
653 • Roumelioti F-M, Sotiriou SK, Katsini V, Chiourea M, Halazonetis TD & Gagos S
654 (2016) Alternative lengthening of human telomeres is a conservative DNA replication
655 process with features of break-induced replication. *EMBO Rep* 17: 1731–1737
656 • Ruis P & Boulton SJ (2021) The end protection problem-an unexpected twist in the
657 tail. *Genes Dev* 35: 1–21
658 • Santos-Pereira JM, García-Rubio ML, González-Aguilera C, Luna R & Aguilera A
659 (2014) A genome-wide function of THSC/TREX-2 at active genes prevents
660 transcription-replication collisions. *Nucleic Acids Res* 42: 12000–12014
661 • Shay JW, Reddel RR & Wright WE (2012) Cancer. Cancer and telomeres--an
662 ALTernative to telomerase. *Science* 336: 1388–1390
663 • Shcheprova Z, Baldi S, Frei SB, Gonnet G & Barral Y (2008) A mechanism for
664 asymmetric segregation of age during yeast budding. *Nature* 454: 728–734
665 • Simon M-N, Churikov D & Géli V (2016) Replication stress as a source of telomere
666 recombination during replicative senescence in Saccharomyces cerevisiae. *FEMS*
667 *Yeast Res* 16
668 • Sinclair DA & Guarente L (1997) Extrachromosomal rDNA circles--a cause of aging
669 in yeast. *Cell* 91: 1033–1042
670 • Teng SC, Chang J, McCowan B & Zakian VA (2000) Telomerase-independent
671 lengthening of yeast telomeres occurs by an abrupt Rad50p-dependent, Rif-inhibited
672 recombinational process. *Mol Cell* 6: 947–952
673 • Teng SC & Zakian VA (1999) Telomere-telomere recombination is an efficient
674 bypass pathway for telomere maintenance in Saccharomyces cerevisiae. *Mol Cell Biol*
675 19: 8083–8093
676 • Tsukamoto Y, Taggart AK & Zakian VA (2001) The role of the Mre11-Rad50-Xrs2
677 complex in telomerase- mediated lengthening of Saccharomyces cerevisiae telomeres.
678 *Curr Biol CB* 11: 1328–1335
679 • Vannier J-B, Pavicic-Kaltenbrunner V, Petalcorin MIR, Ding H & Boulton SJ (2012)
680 RTEL1 dismantles T loops and counteracts telomeric G4-DNA to maintain telomere
681 integrity. *Cell* 149: 795–806
682 • Wellinger RJ, Wolf AJ & Zakian VA (1993) Saccharomyces telomeres acquire single-
683 strand TG1-3 tails late in S phase. *Cell* 72: 51–60
684 • Wright WE, Piatyszek MA, Rainey WE, Byrd W & Shay JW (1996) Telomerase
685 activity in human germline and embryonic tissues and cells. *Dev Genet* 18: 173–179
686 • Yu T-Y, Kao Y & Lin J-J (2014) Telomeric transcripts stimulate telomere
687 recombination to suppress senescence in cells lacking telomerase. *Proc Natl Acad Sci*
688 *U S A* 111: 3377–3382

689 • Zhang T, Zhang Z, Shengzhao G, Li X, Liu H & Zhao Y (2019) Strand break-induced
690 replication fork collapse leads to C-circles, C-overhangs and telomeric recombination.
691 *PLoS Genet* 15: e1007925
692
693
694
695
696
697 **Legend of the Figures**
698
699
700 **Figure 1- Production of telomeric circles during senescence and survivor formation in *S.***
701 ***cerevisiae.***
702 A Schematic of the RCA assay. The Φ29 polymerase produces long telomeric single strand
703 concatemers of the circular DNA in a self-primed reaction.
704 B Schematic of the senescence assay. Senescence assays were performed starting from the
705 spores isolated from the heterozygous telomerase-negative diploids. The spore colonies were
706 inoculated at OD_{600}=0.01 in 15 ml liquid YPD medium. Every 24 hours, the cell density was
707 measured and a new culture was restarted at OD_{600}=0.01. Samples were collected at each
708 time-point for further analyses.
709 C *Upper panel:* senescence curve of a representative *est2*Δ clone. DNA samples were
710 prepared at the indicated time points to analyze telomere length (*middle panel*) and t-circles
711 production (*lower panel and graph*) during senescence and cell immortalization. Telomeres
712 were analyzed by Southern blot of the *XhoI* cut DNA hybridized with a TG_{1-3} probe. The
713 presence of t-circles was monitored by RCA and analyzed by TG_{1-3} probed dot blot. The
714 graph shows signal intensities of the dots measured with the Fiji software (arbitrary units).
715 Similar results were obtained with at least 16 other *est2*Δ clones.
716 D RCA products were resolved by denaturing agarose gel electrophoresis, transferred on a
717 membrane and hybridized with a telomeric TG_{1-3} probe.
718 **E)** Dot blot of the RCA product either treated or not with the Exonuclease VII that degrades
719 linear single-stranded DNA in both the 3' to 5' and 5' to 3' directions (*upper panel*). The
720 membrane was hybridized with a telomeric TG_{1-3} probe. The signal intensities of the dots are
721 shown (*lower graph*).
722
723 **Figure 2- t-circles contain the C-rich telomere strand without subtelomeric Y' sequence.**
724 A Senescence curve of a representative *est2*Δ clone and corresponding dot blot of the RCA
725 product hybridized with the indicated subtelomeric or telomeric probes. t-circle amounts were

726 evaluated based on signal intensity of the dots and were expressed as fold increase over the
727 signal in the absence of Φ29 (*lower graph*).
728 B Senescence curve of a representative *est2*Δ clone (*upper panel*). DNA samples were
729 prepared at the indicated time points to analyze telomere length by Southern blot (*middle*
730 *panel*) and t-circles production by RCA assay performed in the absence of dCTP and
731 dATP.(*lower panel*). The graph shows signal intensities of the dots measured with the Fiji
732 software (arbitrary units).
733
734 **Figure 3- C-circles bind to the NPCs.**
735 A Senescence curves of four *est2*Δ and six *est2*Δ *NIC96-RFP* independent clones used to
736 generate type II survivors for C-circles co-IP experiments. The time when the cells were
737 collected for the Co-IP is indicated by an arrow. The results are shown for one of the 3
738 independent experiments with similar outcomes.
739 B Telomere length and recombination were analyzed by TG_{1-3} probed Southern blot of *XhoI*-
740 digested DNA prepared from samples of the replicative senescence. Two representative
741 clones are shown.
742 C Detection of the t-circles co-immunoprecipitated with Nic96-RFP from the extracts
743 obtained from several type II survivors. The DNA co-immunoprecipitated with Nic96-RFP
744 was amplified by RCA assay, loaded on a dot blot and detected with a telomeric TG_{1-3} probe.
745 The numbers above the blot refer to the growth curves in (A) and correspond to type II
746 survivors produced in independent cultures. The lower panel shows the efficiency of Nic96-
747 RFP IP that was evaluated by western blot with anti-mCherry antibody.
748 D Quantification of the RCA product after co-IP of the C-circles with Nic96-RFP showing
749 the effect of *ADA2* deletion. Dot signal intensities were quantified using the Fiji software and
750 were calculated as the percentage of INPUT that was immunoprecipitated normalized to *est2*Δ
751 signals. Relative signals were calculated by setting the mean of *est2*Δ signals from each
752 independent experiment to 1. Means and s.e.m. of the six independent co-IPs experiments
753 each with 2-6 clones per genotype are shown. Outliers were removed using ROUT robust
754 outlier test. The p-values from one-way ANOVA were adjusted using the Bonferroni's
755 correction for multiple comparisons. *est2*Δ versus *est2*Δ *NIC96-RFP* (p=0,000007), *est2*Δ
756 *NIC96-RFP* versus *est2*Δ *ada2*Δ *NIC96-RFP* (p=0,00012). ***$P<0,0001$.
757 E Quantification of the RCA product after co-IP of the C-circles with Nic96-RFP showing the
758 effect of *SUS1* deletion. Quantification was done as in D. The graph shows means and s.e.m.

759 of the three independent co-IPs with 2-5 clones per genotype. Outliers were removed using
760 ROUT robust outlier test. The p-values from one-way ANOVA were were adjusted using the
761 Bonferroni's correction for multiple comparisons. *est2*Δ versus *est2*Δ *NIC96-RFP* (p=0,002),
762 *est2*Δ versus *est2*Δ *sus1*Δ *NIC96-RFP* (p= 0,0006). **P<0,001, ***P<0,0001.
763
764 **Figure 4- C-circles interact with SAGA/TREX2.**
765 A Senescence curves of two *est2*Δ and two *est2*Δ *ADA2-Myc* clones used to generate type II
766 survivors for Co-IP-RCA. This experiment is representative out of the 4 independent
767 experiments performed during this study.
768 B Telomere length and recombination were analyzed by TG_{1-3}-probed Southern blot of *Xho*I-
769 digested DNA prepared from samples of the replicative senescence.
770 C Detection of the C-circles co-immunoprecipitated with Ada2-Myc in type II survivors. The
771 DNA co-immunoprecipitated with Ada2-Myc was amplified by RCA, loaded on a dot blot
772 and detected with a telomeric TG_{1-3} probe. The numbers above the blot refer to clones in (A)
773 and correspond to type II survivors produced in independent cultures. The lower panel shows
774 the efficiency of Ada2-Myc IP analyzed by western blot with anti-Myc antibody.
775 D Quantification of the dot blot signals in Ada2-Myc co-IP. Dot signals were quantified as in
776 Fig 3D. The graph shows means and s.e.m. from n= 3 independent co-IP experiments each
777 performed with 3-4 independent clones per genotype. The p-value is obtained for the Mann-
778 Whitney two-tailed test (***p= 0. 00000005).
779
780 **Figure 5- Inactivation of SAGA/TREX-2 affect type II telomere recombination.**
781 A Mean senescence profiles of the *est2Δ* (n=7) and *est2Δ sus1Δ* (n=8) clones isolated from
782 the same heterozygous diploid. The error bars are SDs.
783 B Mean senescence profiles of the *est2Δ* (n=10) and *est2Δ sac3Δ* (n=10) clones isolated from
784 one heterozygous diploid. The error bars are SDs.
785 C Duration of the short telomere-induced crisis of the clones analyzed in A). The crisis period
786 was determined as the number of days the cell population stayed arrested without notable
787 increase in cell density. The average crisis period is plotted for each genotype. *est2*Δ *ada2*Δ
788 data are from (Churikov et al 2016) and are shown for comparison. The error bars are SD of n
789 independent clones. *est2Δ* (n=17), *est2Δ ada2Δ* (n=11), *est2Δ sus1Δ* (n=8) and *est2Δ sac3Δ*
790 (n=10). The p values are from two-tailed Student's tests. p=0,000087 for *ada2*Δ, p=0,047 for
791 *sus1*Δ, p=0,049 for *ada2*Δ.*P<0,05, ***P<0,0001

792 D Frequencies of the telomerase-independent survivor types formed by the clones shown in
793 A.
794
795 **Figure 6- The nuclear diffusion barrier promotes type II recombination.**
796 A Mean senescence profiles of the *est2Δ* (n=10) and *est2Δ shs1Δ* (n=16) clones. The error
797 bars are SDs.
798 **B** Mean senescence profiles of the *est1Δ* (n=6) and *est1Δ bud6Δ* (n=7) clones. Est1, similarly
799 to Est2, is essential for telomere maintenance. *est1*Δ has been used in this experiment instead
800 of *est2*Δ because *EST2* and *BUD6* genes are linked on chromosome XII. The error bars are
801 SDs.
802 C Duration of the short telomere-induced crisis for the clones analysed in A) and B). The
803 crisis period was determined as the number of days the cell population stayed arrested without
804 notable increase in cell density. The average crisis period is plotted for each genotype. The
805 error bars are SDs of n independent clones: *est2Δ* (n=10), *est2Δ shs1Δ* (n=16), *est1Δ* (n=6)
806 and *est1Δ bud6Δ* (n=7) . P values are from two-tailed Student's tests (*p=0.014).
807 D Frequencies of the survivor types formed by the clones used in the senescence assays
808 shown in A and B.
809
810 **Figure 7- Model of type II telomere recombination that relies on telomeric circles.** C-
811 circles localize at the NPCs in a SAGA/TREX2-dependent process. We previously showed
812 that eroded telomeres also localize to the NPCs in a SUMO and Slx5/Slx8-dependent manner,
813 which favors type II recombination (Churikov et al., 2016). Co-localization of the C-circles
814 and eroded telomeres at NPCs may favor SSA between the telomeric 3'-overhang and the
815 telomeric circles, thereby promoting telomere elongation. In this scheme C-circles serve as a
816 template for elongation of the G-strand of telomeres which is followed by synthesis of the
817 complementary strand by Polα (not shown).
818 .
819
820

821 **EXPANDED FIGURE LEGENDS**
822
823 **Figure EV1: C-circles are not produced in the absence of Rad59.**
824 **(A)** Analyses of the telomeres and C-circles in *rad59Δ est2Δ* cells during senescence.
825 Senescence curve of one representative *rad59Δ est2*Δ clone is shown (*middle panel*). At the
826 indicated time points, DNA was extracted and analyzed by telomere Southern blot (*upper*
827 *panel*) and RCA assay (*lower panel and graph*) both hybridized with a TG_{1-3} probe. The
828 abundance of C-circles was evaluated based on the signal intensity of the dots (*lower graph*).
829 Similar results were obtained with 2 independent *est2*Δ *rad59*Δ clones.
830 **(B)** Analyses of the telomeres and C-circles in *rad51Δ est2Δ* cells during senescence. *Middle*
831 *panel*: senescence curve of one representative *rad51Δ est2Δ* clone. At the indicated time
832 points DNA was extracted and analyzed by Southern blot (*upper panel*) and RCA assay
833 (*lower panel*), both hybridized with a TG_{1-3} probe. The abundance of C-circles was evaluated
834 based on the signal intensity of the dots (*lower graph*).
835
836 **Figure EV2**: **C-circles do not contain RNA-DNA hybrid.**
837 **(A)** Senescence curve of one *est2Δ* clone (*upper panel*). DNA extracted at the indicated time
838 points was treated with 0.5mg/ml RNaseA before RCA assay. The dot blot was hybridized
839 with a telomeric TG_{1-3} probe (*lower panel*).
840 **(B)** Senescence curve of one *est2Δ* clone (*upper panel*). DNA extracted at the indicated time
841 points was treated with 5U of RNaseH1 before RCA assay. The dot blot was hybridized with
842 a specific telomeric TG_{1-3} probe (*middle panel*). The abundance of t-circles evaluated based
843 on the signal intensity of the dots (minus the intensity of the signal in the absence of Φ29)
844 (*lower graph*).
845 **(C)** *Upper panel*: senescence curve of one representative *pGal-RNH1 est2Δ* clone grown in
846 the presence of galactose. DNA samples were prepared at the indicated time points to analyze
847 telomere length by TG_{1-3} probed Southern blot of the *Xho*I cut DNA (*middle panel*) and t-
848 circle production by RCA followed by dot blot probed with a telomeric TG_{1-3} probe (*lower*
849 *panel*). The abundance of t-circles was evaluated based on the signal intensity of the dots
850 (*lower graph*). Two *pGal-RNH1 est2Δ* clones were analyzed with similar results.
851
852

853

854 **Figure EV3. Association of the C-circles with NPCs is SAGA/TREX2-dependent.**

855 **(A)** Interaction between the C-circles and Nic-96-RFP is decreased in the absence of Ada2
856 *(related to Fig. 3D)*. The DNA co-immunoprecipitated with Nic96-RFP was amplified by
857 RCA assay, loaded on a dot blot and detected with a telomeric TG_{1-3} probe. The genotypes of
858 the survivors are indicated, and the numbers refer to independent clones. Dot signals were
859 quantified using the Fiji software and are represented as the percentage of INPUT that was
860 immunoprecipitated after normalization to the *est2*Δ signals set to one.

861 **(B)** Interaction between the C-circles and Nic96-RFP is decreased in the absence of Sus1
862 *(related to Fig. 3E)*. The DNA co-immunoprecipitated with Nic96-RFP was amplified by
863 RCA assay, loaded on a dot blot and detected with a telomeric TG_{1-3} probe. The genotypes of
864 the survivors are indicated, and the numbers refer to independent cultures. Dot signals were
865 quantified as described in A.

866 **(C)** Analysis of the RCA product by denaturing agarose gel electrophoresis *(related to Fig.4)*.
867 Whole cell extracts were prepared from the indicated strains. Numbers correspond to
868 independent type II survivors. The DNA co-immunoprecipitated with Ada2-Myc was
869 amplified by RCA. The RCA product from the Co-IP and INPUT samples was resolved by
870 denaturing agarose gel electrophoresis and hybridized with a telomeric TG_{1-3} probe.

871 **(D)** RCA of the C-circles co-immunoprecipitated with Sac3-Myc. Type II survivors derived
872 from senescence of *est2*Δ and *est2*Δ *SAC3*-myc clones were isolated. Whole cell extracts from
873 the indicated strains were IP with anti-Myc antibodies, and the co-immunoprecipitated DNA
874 was amplified by RCA. Products of the RCA were loaded on a dot blot and detected with a
875 telomeric TG_{1-3} probe. Dot signals were quantified as described in A. The lower panel shows
876 the efficiency of Sac3-Myc IP analyzed by western blot with anti-Myc antibodies. These
877 results are representative of two independent experiments.

878

879 **Figure EV4. TERRA transcription and telomere localization in *est2Δ ada2Δ* cells.**

880 **(A)** Senescence curves of the *est2Δ* and *est2Δ ada2Δ* clones, one of each. Cell populations
881 were maintained in the exponential phase of growth by diluting the cultures to OD_{600}=0.01 as
882 soon as they reached OD_{600}=0.8. The generation time is shown as a function of the number of
883 population doublings.

884 **(B)** TERRA levels at telomere 15L (upper graph) and 10R (lower graph) during replicative
885 senescence in *est2Δ* and *est2Δ ada2Δ* clones shown in (A). TERRA levels were analyzed by

886 qPCR after reverse transcription of the total RNA. TERRA levels were normalized to the
887 *ACT1* RNA levels and are represented as fold change relative to the first time point of the
888 *est2*Δ control that is set to one for each telomere. Two technical replicates are shown for each
889 genotype.
890 **(C)** Localization of eroded telomeres in *est2*Δ *ada2*Δ cells during senescence and at crisis.
891 Eroded telomeres were detected as foci containing Cdc13-YFP and Rad52-RFP. Percentages
892 of the Cdc13-YFP/Rad52-RFP foci that co-localize with CFP-Nup49 are shown in the
893 *nup133ΔN* background in which NPCs cluster at one side of the nucleus (Charifi *et al*, 2021).
894 Three independent *est2*Δ *ada2*Δ clones were analyzed. The error bars are SDs.
895
896 **Figure EV5. Type II recombination is prevented at 37°C.**
897 **(A, B)** (A) Left *panel*: An entire *est2*Δ spore colony was diluted in YPD and the cell
898 suspension split to inoculate two cultures at OD_{600}=0.01. One was grown at 30°C and the
899 other at 37°C. The senescence curves are shown. *Right Panel*: DNA samples were prepared at
900 the different time points, and telomere length analysis was performed by TG_{1-3} probed
901 Southern blot after *XhoI* digestion. **(B)** Same as in **(A)**, with a second independently isolated
902 clone.
903
904

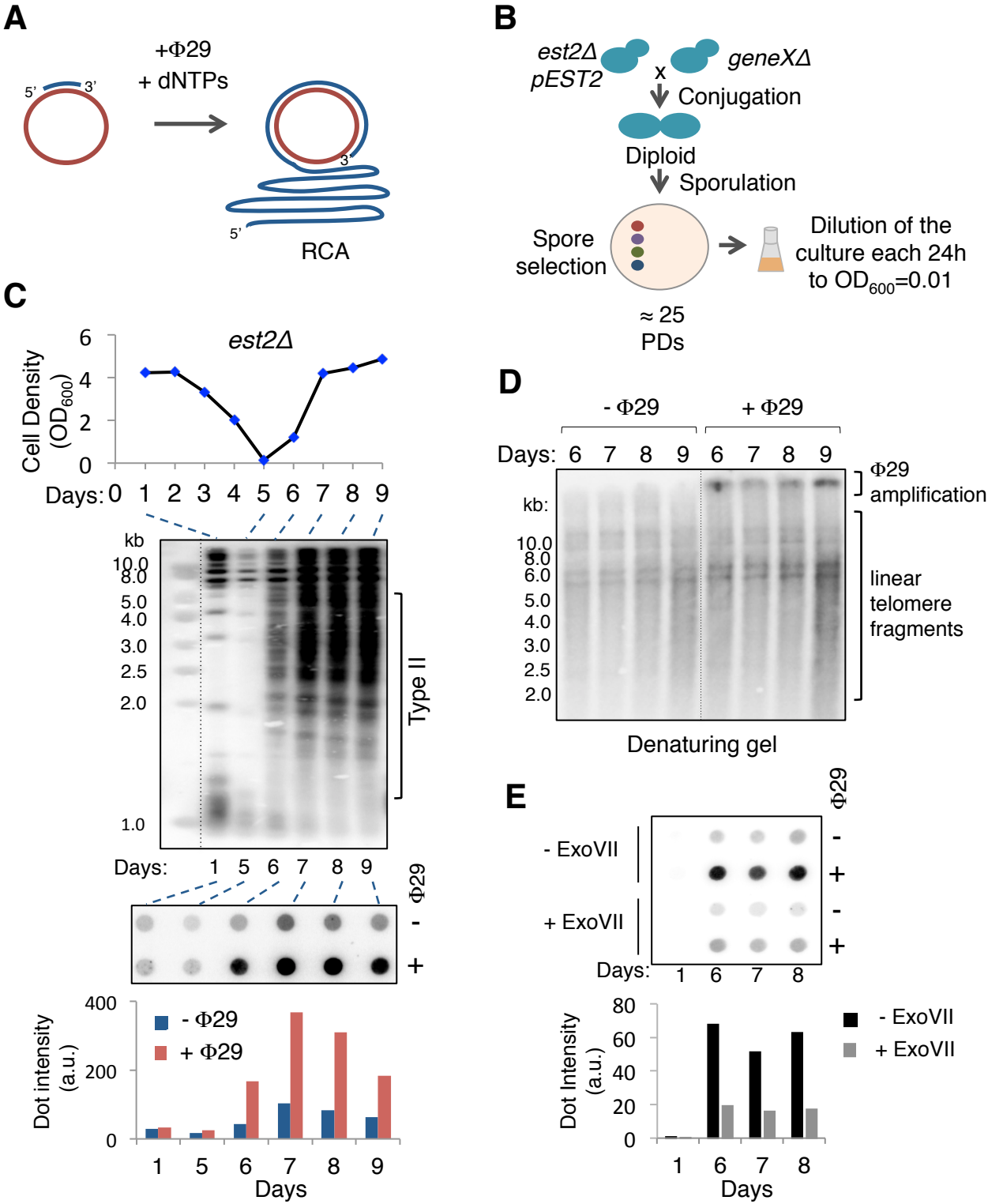

Aguilera et al. Figure 1

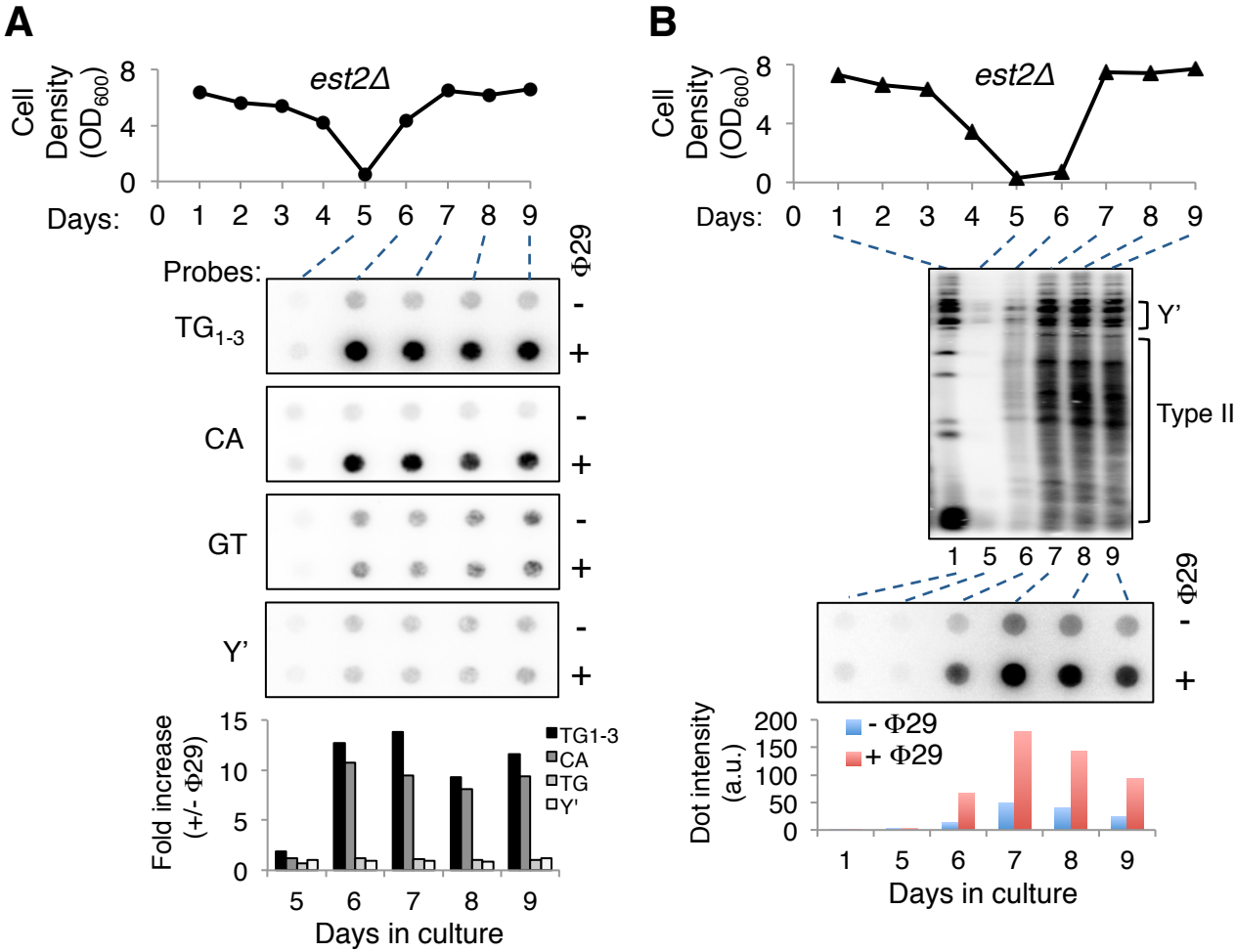

Aguilera et al. Figure 2

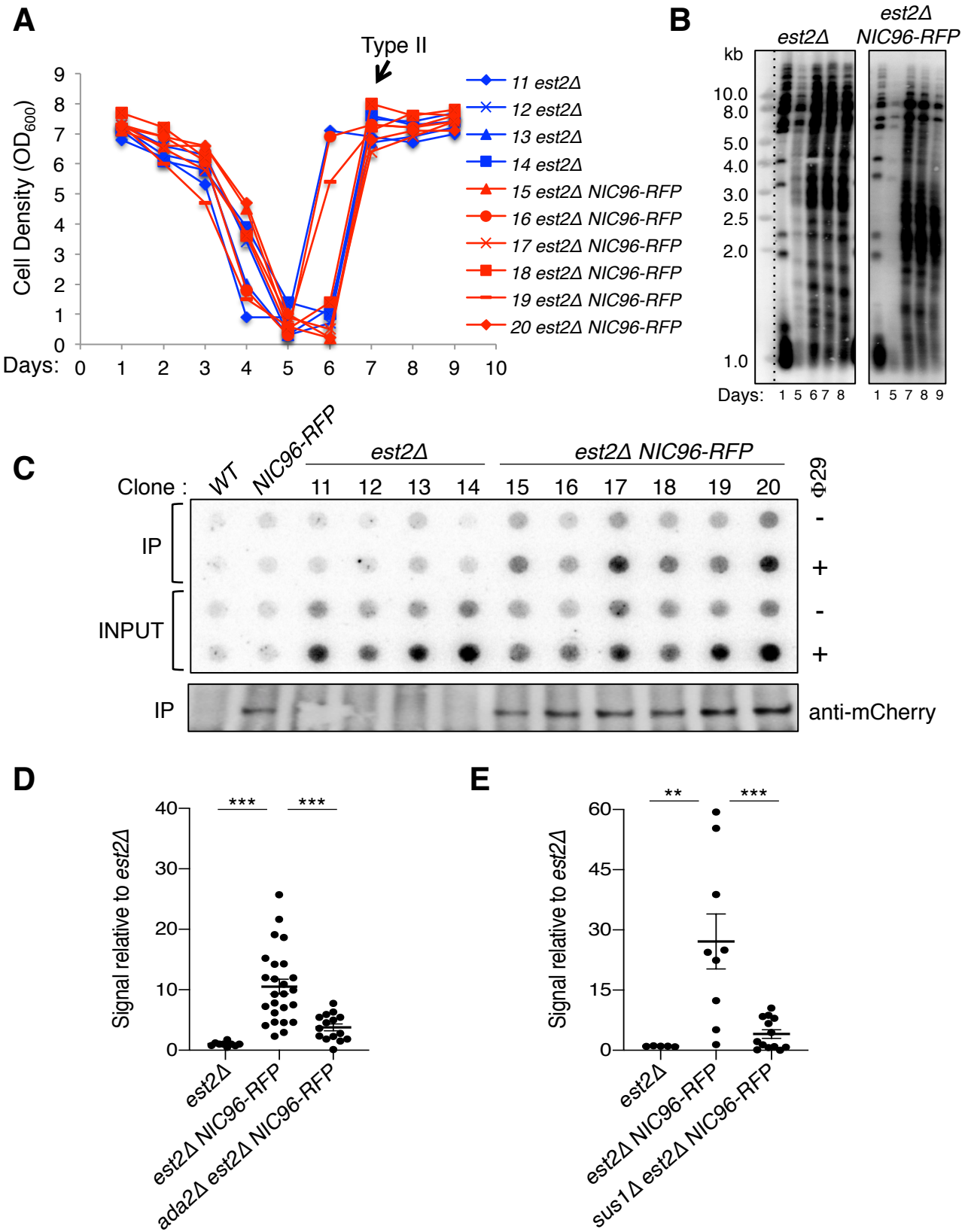

Aguilera et al. Figure 3

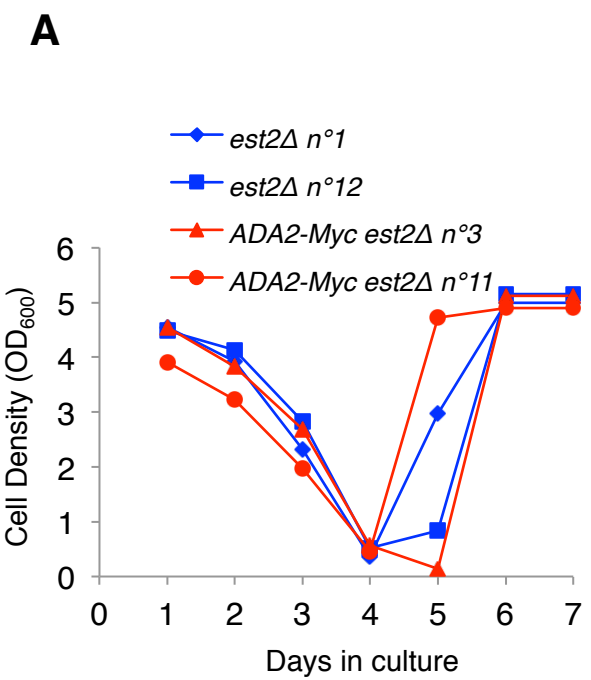

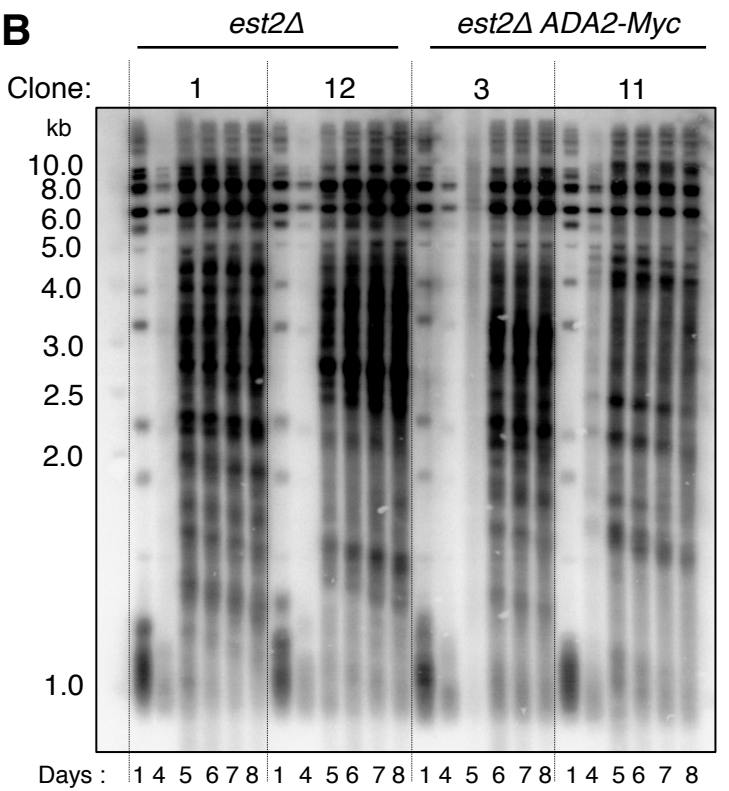

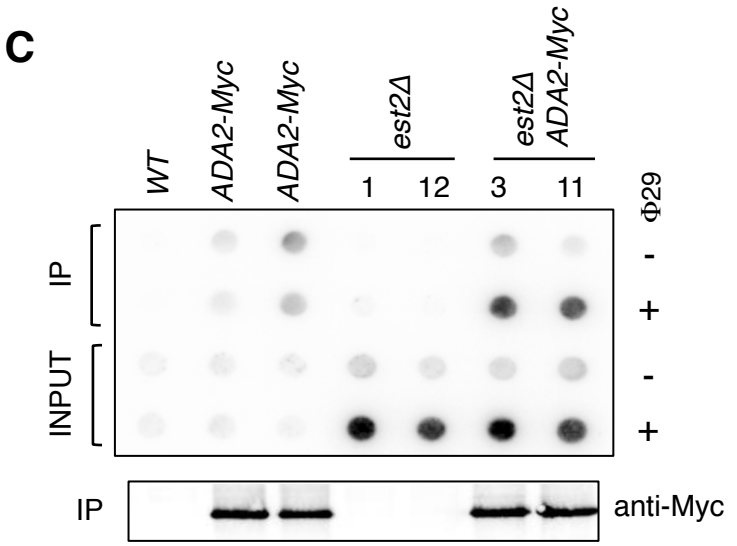

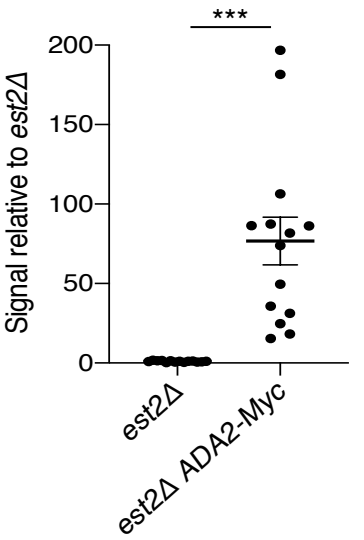

Aguilera et al. Figure 4

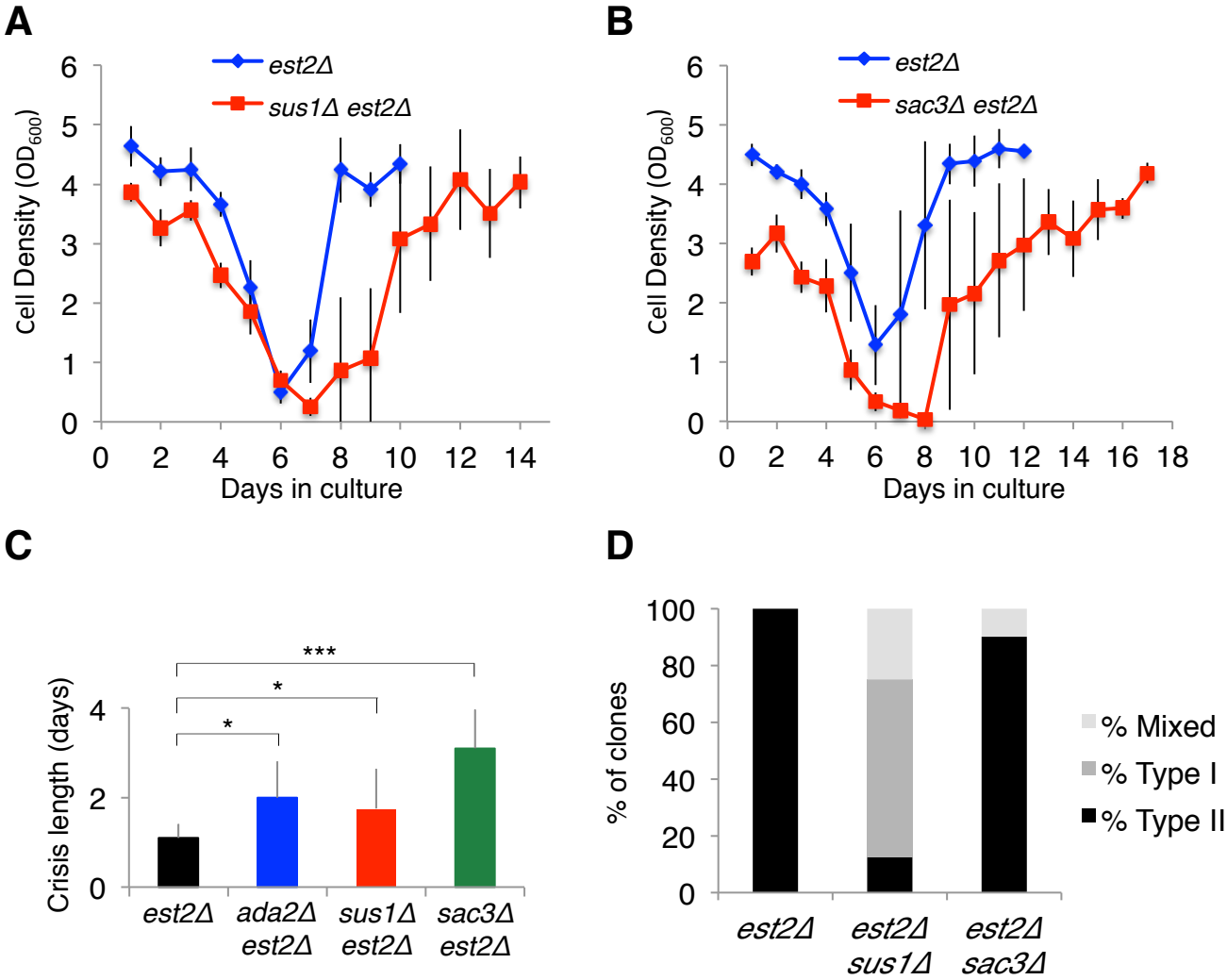

Aguilera et al. Figure 5

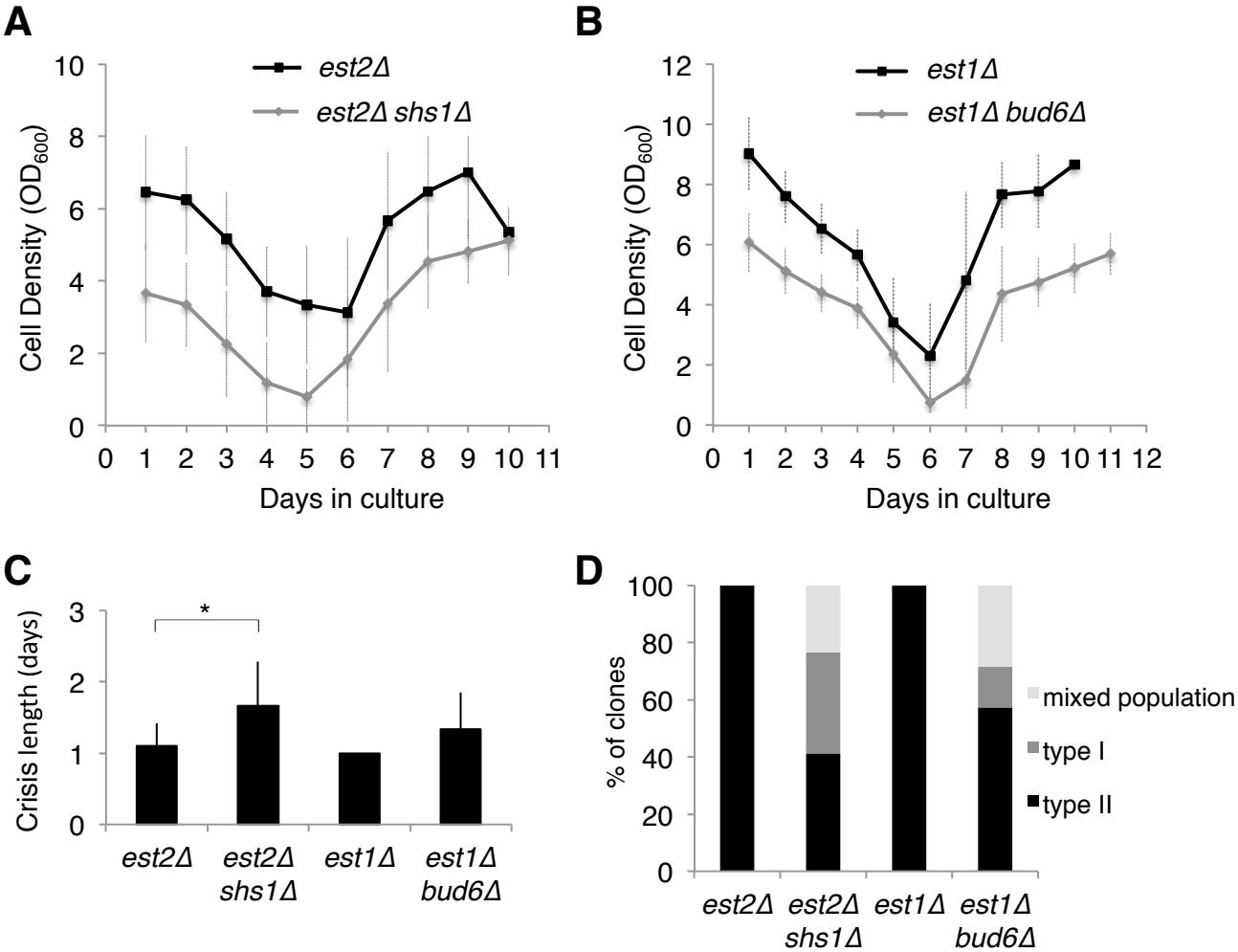

Aguilera et al. Figure 6

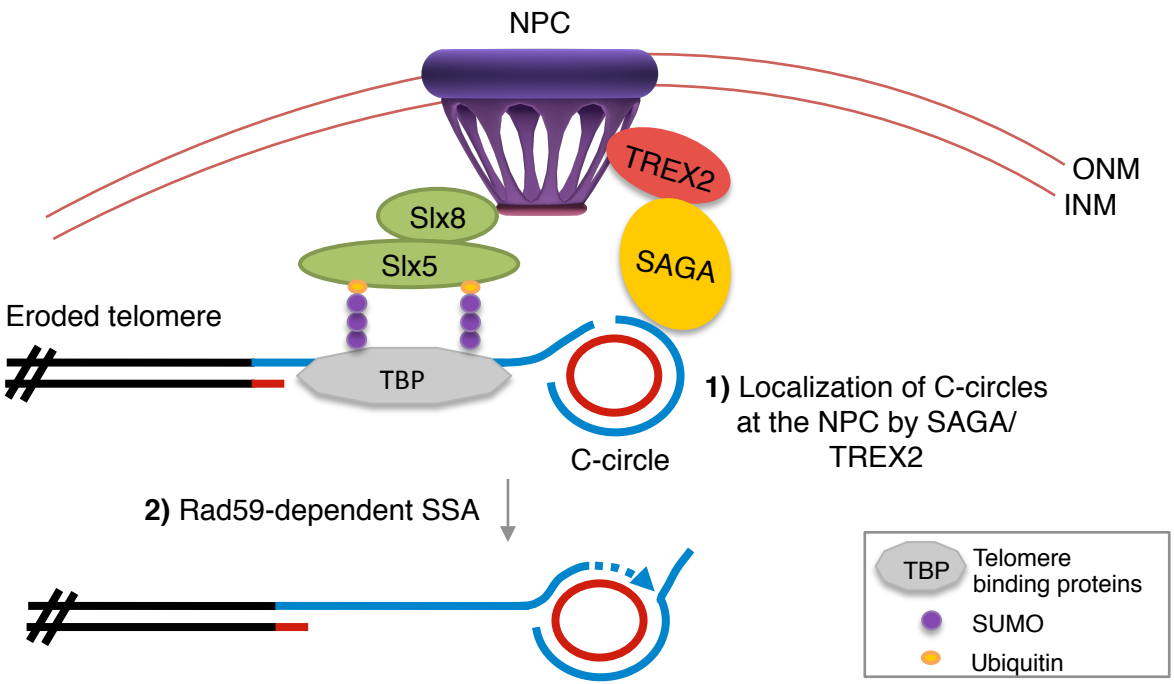

Aguilera et al. Figure 7

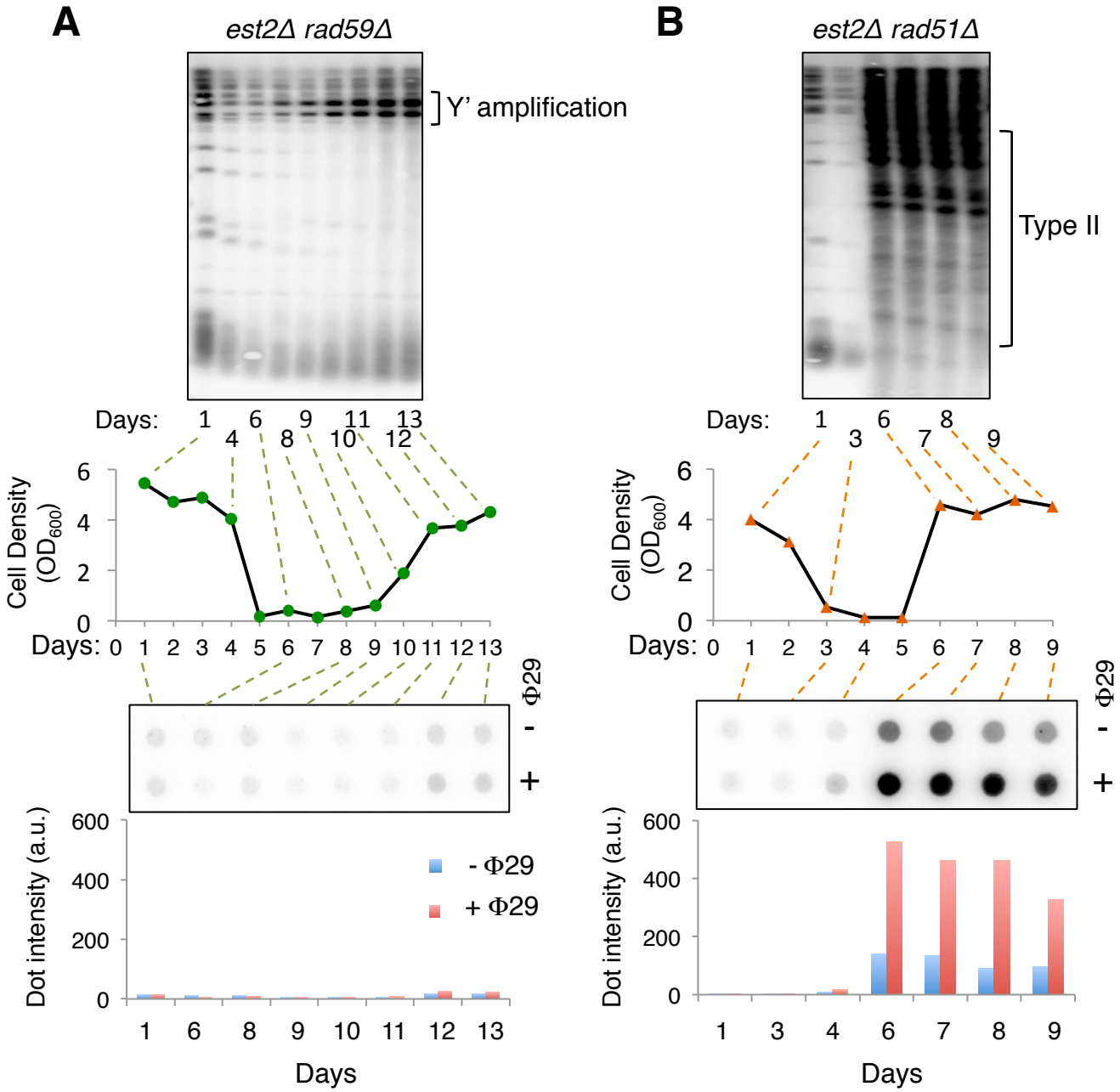

Aguilera et al. Figure EV1

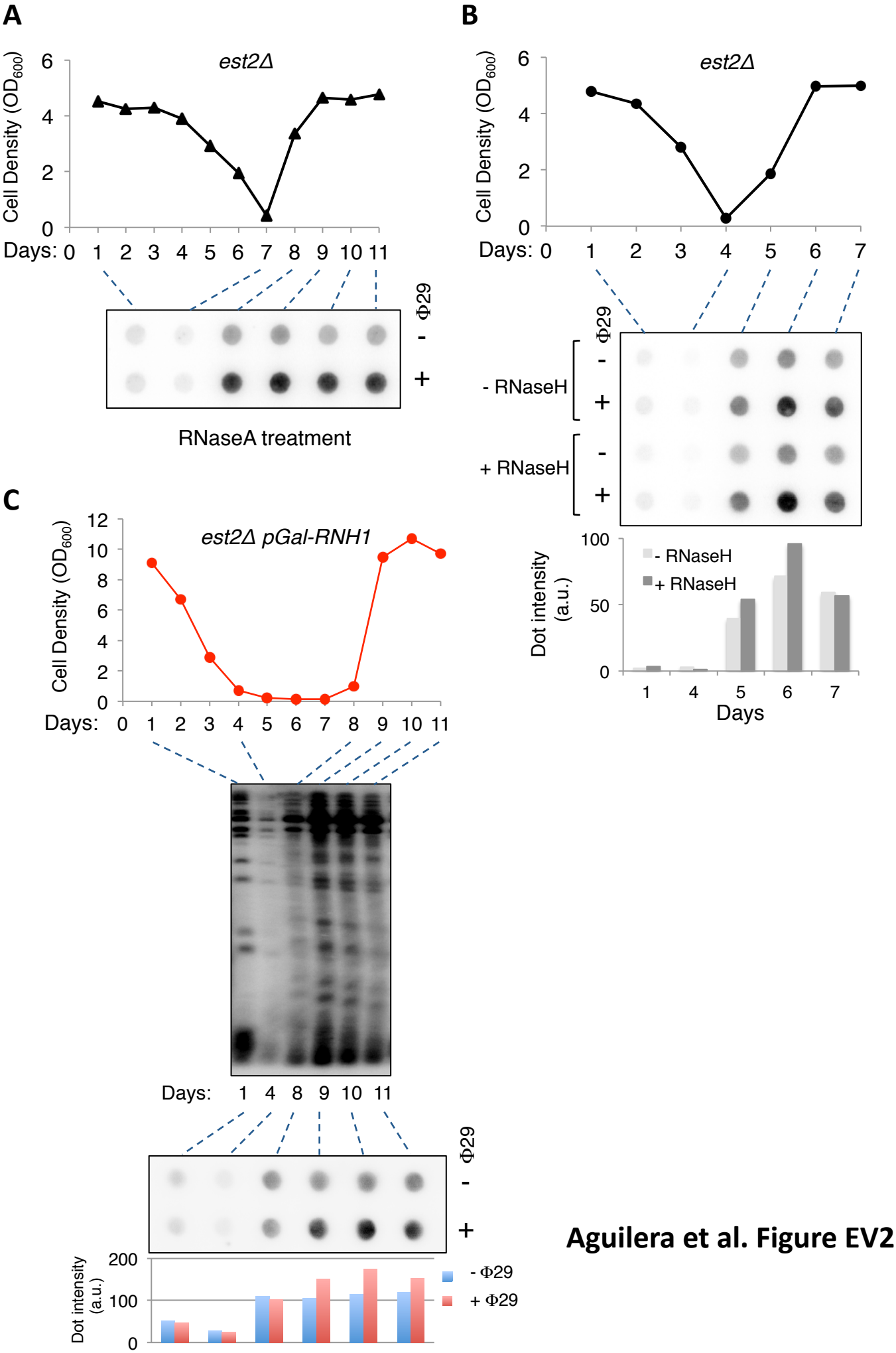

Aguilera et al. Figure EV2

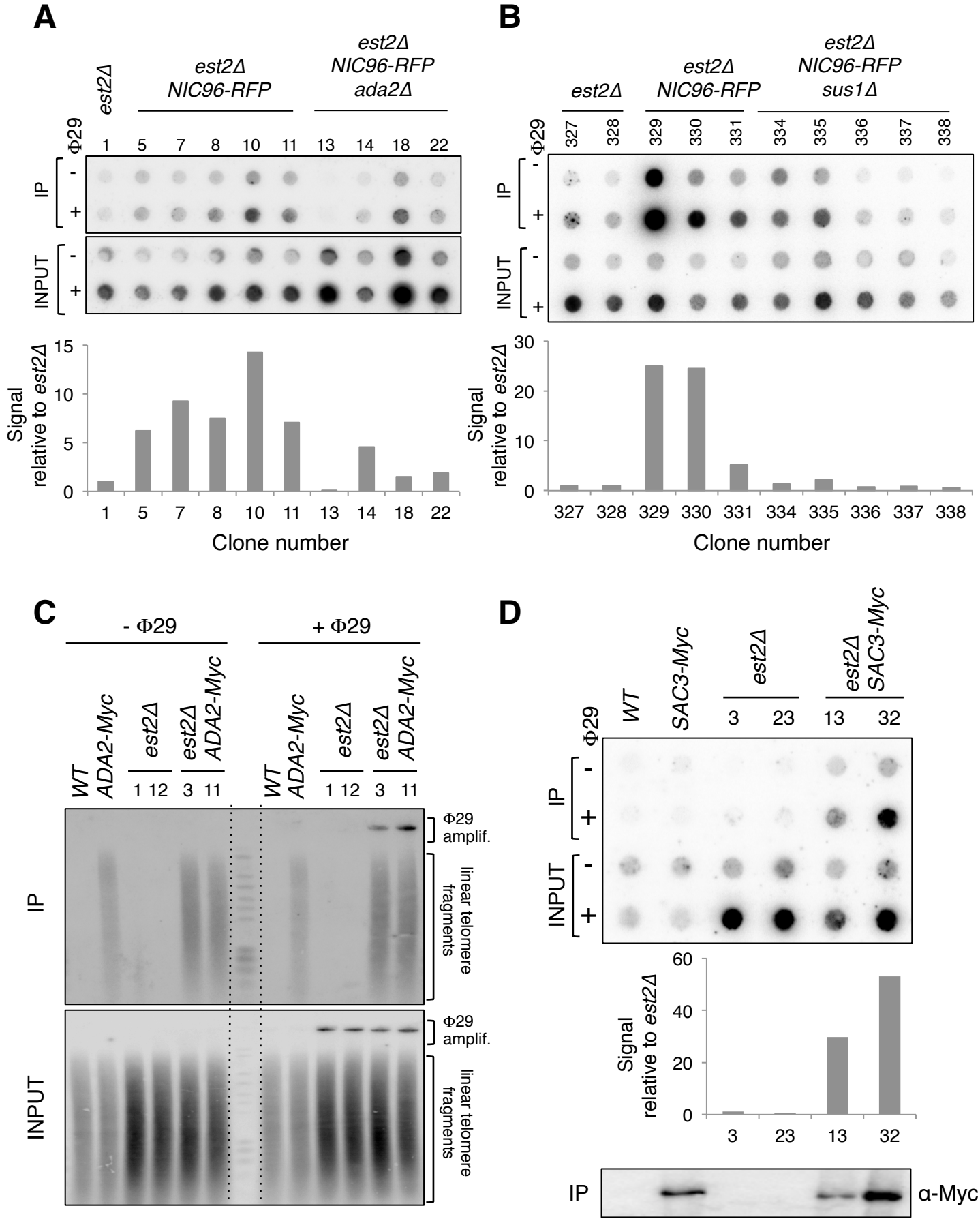

Aguilera et al. Figure EV3

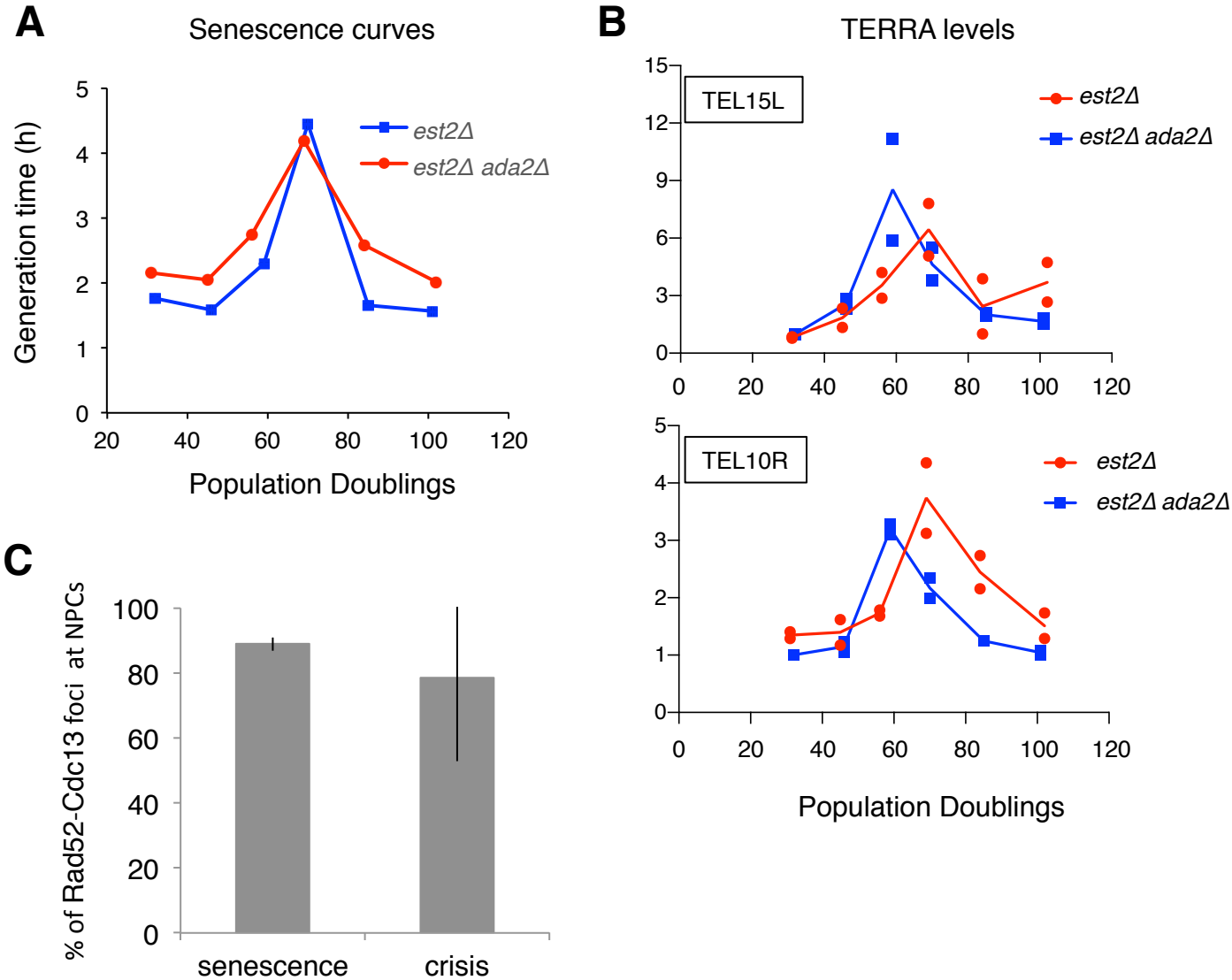

Aguilera et al. Figure EV4

A

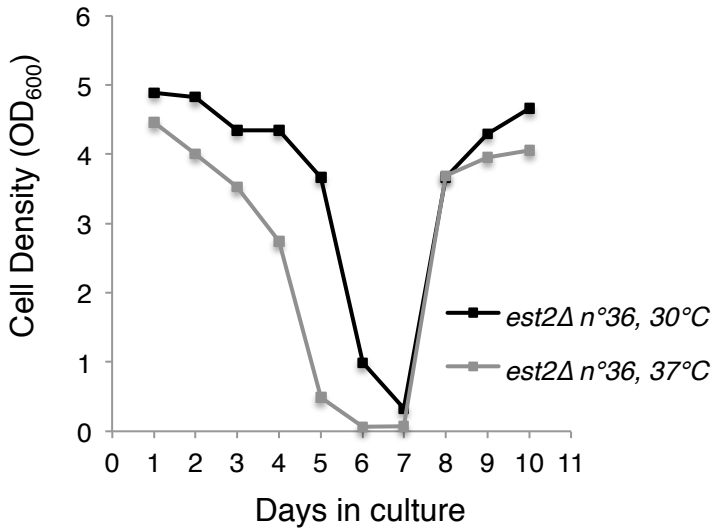

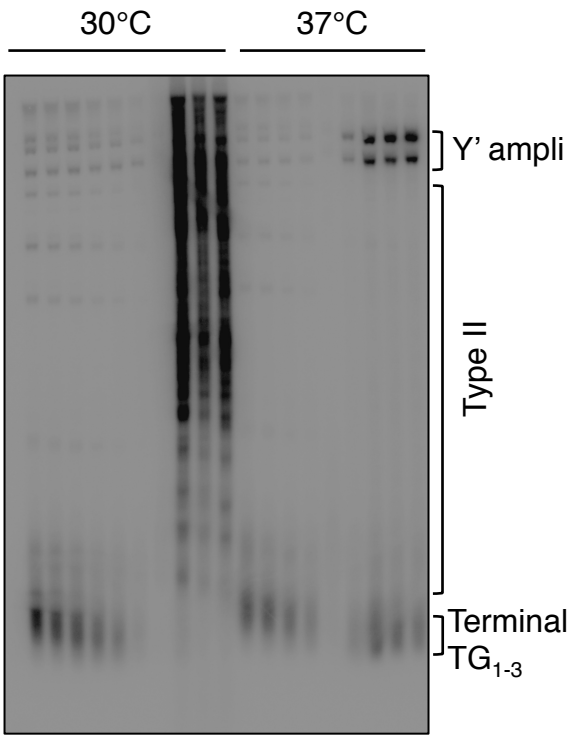

B

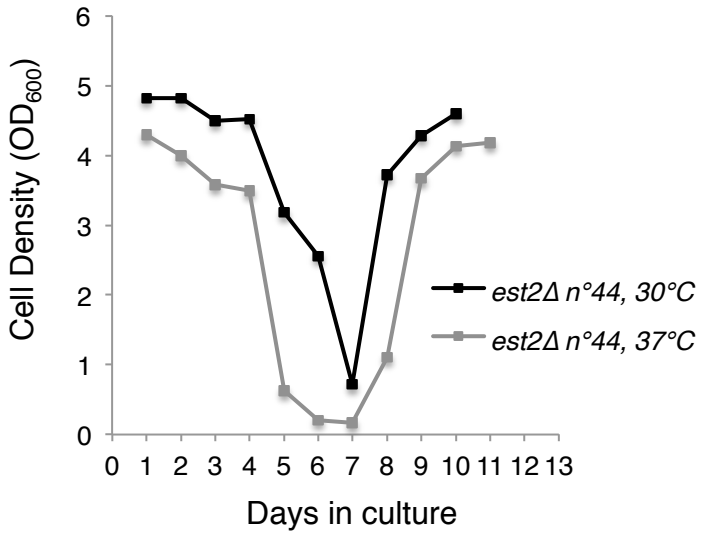

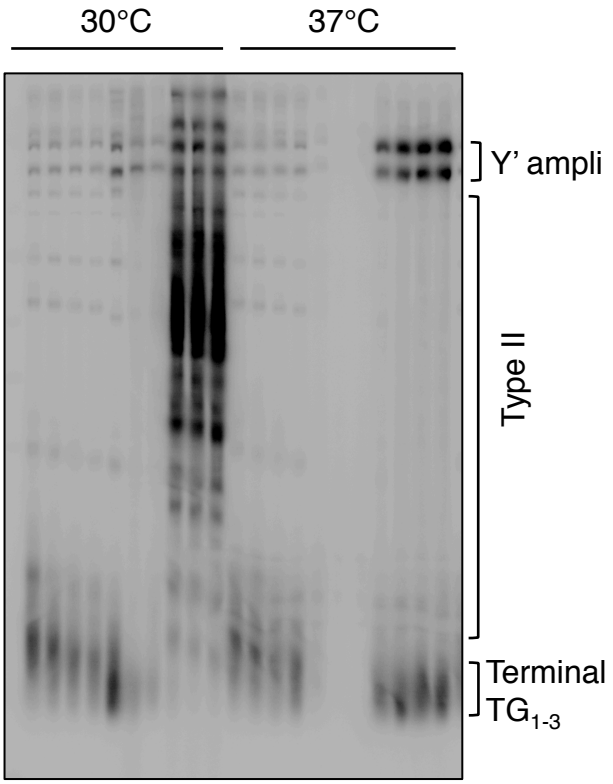

Aguilera et al. Figure EV5